CAVITATION

AND

PRESSURE DISTRIBUTION

Head Forms at Zero Angle of Yaw

By

HUNTER ROUSE

and

JOHN S. McNOWN

State University of Iowa
Studies in Engineering
Bulletin 32

Published by the State University of Iowa

No. 420

CAVITATION

AND

PRESSURE DISTRIBUTION

Head Forms at Zero Angle of Yaw

By

HUNTER ROUSE
Director

and

JOHN S. McNOWN
Research Engineer

Iowa Institute of Hydraulic Research

Publication sponsored by the
Office of Naval Research
Contract N8onr-500

Published by the State University of Iowa
Iowa City
1948

CAVITATION AND PRESSURE DISTRIBUTION

Head Forms at Zero Angle of Yaw

by

Hunter Rouse and John S. McNown

Iowa Institute of Hydraulic Research
State University of Iowa
Iowa City

I. Introduction

Early in the fall of 1943 the Iowa Institute of Hydraulic Research undertook the design and fabrication of a variable-pressure water tunnel, for which a grant of $5000 had been made by the University. Although ultimately intended for Institute research in the post-war period, the equipment was constructed during the war in order that it would be available for eventual studies requested by the Armed Forces. The shortages of necessary material and equipment, combined with a relatively low priority rating, served to make the erection of the tunnel a difficult matter, to say the least. As the tunnel neared completion, however, its immediate use for the study of the pressure distribution around various body forms was requested by the David Taylor Model Basin of the U. S. Navy, and in June 1944 Contract sr-1353 was arranged for this purpose by the National Defense Research Committee of the Office of Scientific Research and Development.

About a year later the pressing need for direct government sponsorship of large-scale research had decreased to the point that most of the NDRC research contracts were being terminated. Since the investigation was far from complete and the results were considered of fundamental importance, in May 1945 sponsorship of this study was transferred to the Bureau of Ships of the U. S. Navy, Contract NObs-24084, under the direct supervision of the David Taylor Model Basin. This arrangement continued in effect until December 1947, at which time sponsorship was assumed by the Office of Naval Research under Contract N7onr-495. A number of progress and summary reports describing various phases of the

study have been submitted for limited distribution — namely, NDRC Reports 6.1-sr1353-2190 to -2196, Bureau of Ships Contract NObs-24084 Reports 1-10 and 12-14, and Office of Naval Research Contract N7onr-495 Report 1. The material presented in this bulletin represents a comprehensive summary of the experiments described in these reports. In addition a detailed study of the water-tunnel characteristics and proper operative procedure has been made and is presented herewith.

The original request for this investigation was a natural outgrowth of the need for systematic data on the distribution of pressure in flow around various bodies, particularly under conditions leading to cavitation, information which is desirable for the design of a wide variety of Navy equipment. Ultimately the study is to include data for two- and three-dimensional head and tail forms at various angles of yaw. The first phase of the study, namely the investigation of three-dimensional head forms at zero angle of yaw, is described herein. Three general geometric series have been studied — rounded, ellipsoidal, and conical — together with other related forms. The data obtained have been systematized to yield information for a wide variety of geometrical forms either directly or by interpolation. Whenever possible, analytical methods have been used to corroborate the experimental data and to provide a reliable means of generalizing the results.

II. Description of Experimental Equipment

The water tunnel as a research tool has been developed specifically for the purpose of studying cavitation resulting from relative motion between a solid boundary and water. Since a given degree of cavitation may be achieved by varying either the velocity or the pressure, means are usually provided whereby the rate of flow and intensity of pressure can be controlled independently. As its name implies, the water tunnel is the water counterpart of the wind tunnel, a strong resemblance between design features of the two types of equipment being readily apparent.

A photograph of the test section of the water tunnel at the Iowa Institute of Hydraulic Research is shown in Fig. 1, and a longitudinal section in Fig. 2. The axis of the tunnel proper has the form of a vertical rectangle 11 feet high and 14 feet wide, the test section being located at eye height above the first floor of the Hydraulics Laboratory of the Institute, and the pump foundation resting on

the floor of the first basement. The tunnel diameter varies gradually from 2 feet at the pump to 3 feet just before the bell inlet to the test section, and beyond the test section it again varies gradually from about $1\frac{1}{4}$ feet to 2 feet at the pump intake. The tunnel walls are of $\frac{3}{16}$-inch steel plate welded to $\frac{1}{2}$-inch flanges, the three miter corners containing louvers of $\frac{1}{8}$-inch plate. Quarter-inch live-rubber gaskets serve to seal all bolted joints. Except for the two interchangeable test sections, the entire inner surface of the tunnel is protected against corrosion by two coats of Bitumastic No. 50 paint.

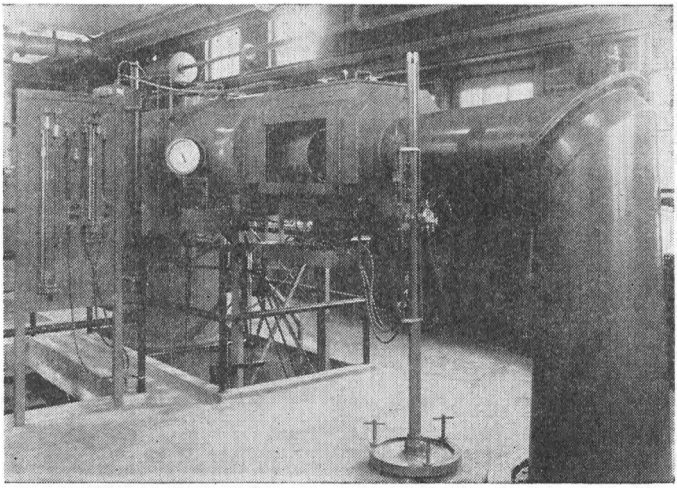

FIG. 1. PHOTOGRAPH OF TEST SECTION, INCLUDING CONTROLS AND GAGES.

The axial-flow pump is a standard product of the Fairbanks-Morse Company, with bronze impeller, steel shaft, and cast-iron casing. Owing to the lack of sufficient direct-current power for a variable-speed electric drive, an 80-horsepower Continental gasoline engine was purchased for this purpose, and connected to the pump shaft by means of V-belts and sheaves yielding a 2:1 speed reduction. The clutch and throttle were provided with remote-control extensions to the immediate vicinity of the test section. At the maximum practicable engine speed of 1500 rpm the pump yields a flow of some 35 cubic feet of water per second; at its idling speed of 350 rpm the flow is about 8 cubic feet per second.

Two interchangeable test sections were designed: one of the open-throat type, shown in Figs. 1 and 2, in which the jet from the

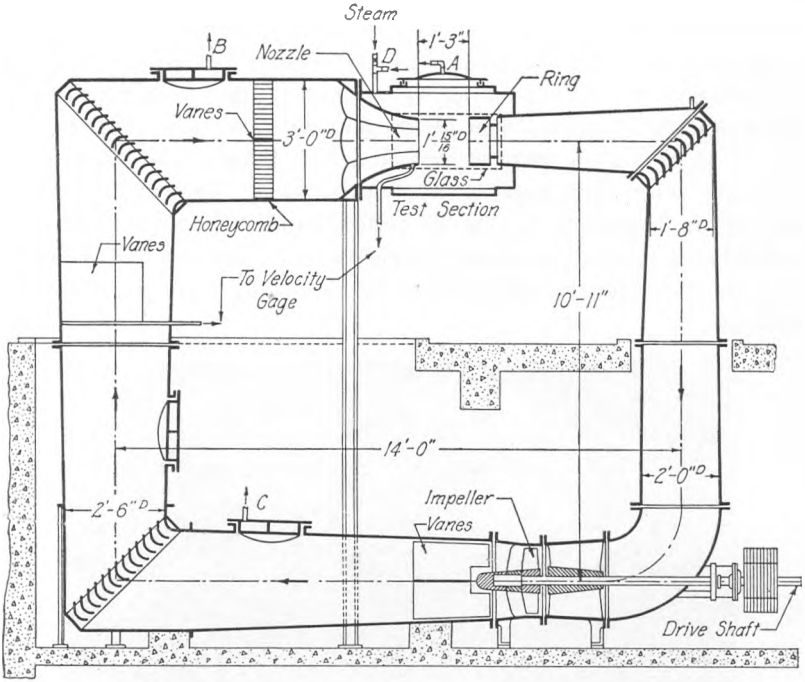

FIG. 2. VERTICAL SECTION THROUGH WATER TUNNEL.

nozzle is unconfined for about one diameter; and one of the closed-throat type, in which the boundary is continuous. Each throat has a cross-sectional area of 1 square foot, so that the normal operating range of the system yields throat velocities varying from 8 to 35 feet per second. Both for ease of construction and for proper guidance of the approaching flow in the two instances, the base of the nozzle within the 3-foot approach section was made in the shape of an octagonal pyramid, the matching ends of the interchangeable sections then being followed by smooth transitions to the circular cross section of the open throat and the square cross section of the closed throat, respectively. The octagonal housing for the open-throat section contains provisions for 4 windows of $\frac{3}{4}$-inch tempered plate glass; only the two side windows have been installed, however, the top and bottom openings being covered with steel plates permitting ready access to the interior. The closed-throat section also contains four openings for either windows or removable covers. The interiors of both sections were given 4 coats of light grey Ucilon paint.

To provide a means of measuring the rate of flow in a manner essentially independent of disturbances produced by bodies in the test section, a horizontal tube with 9 interconnected $\frac{1}{32}$-inch stagnation piezometers was installed in the vertical leg of the tunnel leading to the test section, and a single wall piezometer was placed in the lip of the nozzle. The differential pressure between the stagnation piezometers and the nozzle piezometer, as read on a mercury manometer, is proportional to the square of the rate of flow, the installation being similar in effect to a Venturi meter. Calibration against Pitot-tube traverses of the jet permits this meter to provide a sensitive indication of the velocity head at the test section. A single reading suffices, as one leg of the U-tube gage contains a pot with a cross section some 50 times greater than the bore of the tube, a small correction factor providing for deflection of the mercury in the enlarged section. A wire loop and vernier attached to the gage rider permit readings to the nearest 0.001 foot.

As a means of controlling the pressure intensity within the sealed tunnel, a vacuum pump, auxiliary tank, and secondary circulating system were installed as shown in Fig. 3. The vacuum pump is

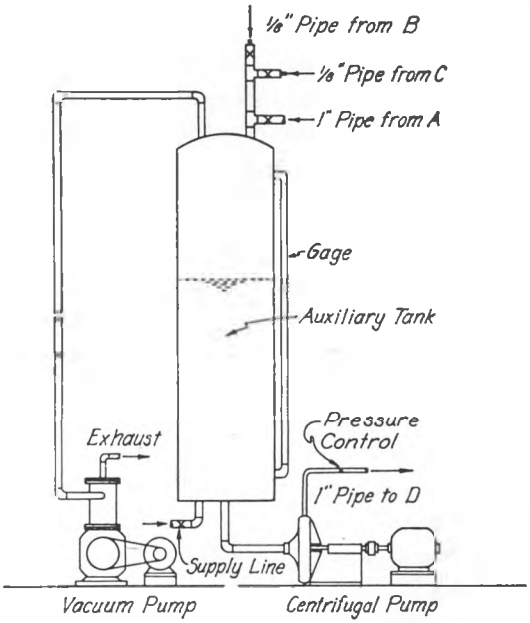

FIG. 3. VACUUM PUMP AND AUXILIARY SYSTEM FOR CONTROLLING PRESSURE.

connected directly to the top of the 1-foot-diameter auxiliary tank where a minimum absolute pressure head of 3 feet of water can be maintained. A double line between the tank and tunnel, a pump, and appropriate valving permit both regulation of the pressure within the tunnel relative to that in the small tank, and continuous removal of air from the test section to the auxiliary tank. By this means it is possible to produce at the axis of the test section a pressure head varying from +30 to —30 feet of water. In order to measure the pressure head at the jet axis during tests without introducing an instrument which would disturb the flow, a brass plate containing 3 piezometers on 3-inch centers was secured to one longitudinal wall of the test section. The three piezometers were interconnected, a common lead passing to a mercury U-tube similar to that for the velocity gage except that one arm of this manometer is open to the atmosphere. All pressure readings are subject to corrections for variations in atmospheric pressure as determined by a precision barometer. The head reading is referred to the elevation of the jet axis by means of a zero reading on an open container of water having the proper surface level.

To permit heating of the water in the tunnel so as to extend the Reynolds-number range over which the tunnel can be operated, provisions were made to supply steam directly to the water in the tunnel. For this purpose a line was connected from the steam lines of the heating plant to the tunnel, utilizing the same inlet as for the pressure-regulation system (see Fig. 2). In terms of the 1-inch bodies under study, Reynolds numbers from 5×10^4 to 5×10^5 can thus be obtained.

The initial tests requested by the David Taylor Model Basin involved a systematic series of bodies of revolution encompassing the range of head forms of interest in the design of underwater projectiles. These tests were to include the measurement of pressure distribution and the photography of the vapor pocket for each form at various degrees of cavitation. Since every body tested possessed a cylindrical shank of considerable length, the several heads were so constructed that they could be mounted interchangeably at the end of a fixed shaft of the same diameter. As shown in Fig. 4, the shaft consists of a brass sleeve machined to an outside diameter of 1 inch and supported by $\frac{1}{8}$-inch brass gusset plates brazed to streamlined cross struts, which in turn contain $\frac{3}{8}$-inch leveling screws passing through clips on the outlet wall of the test

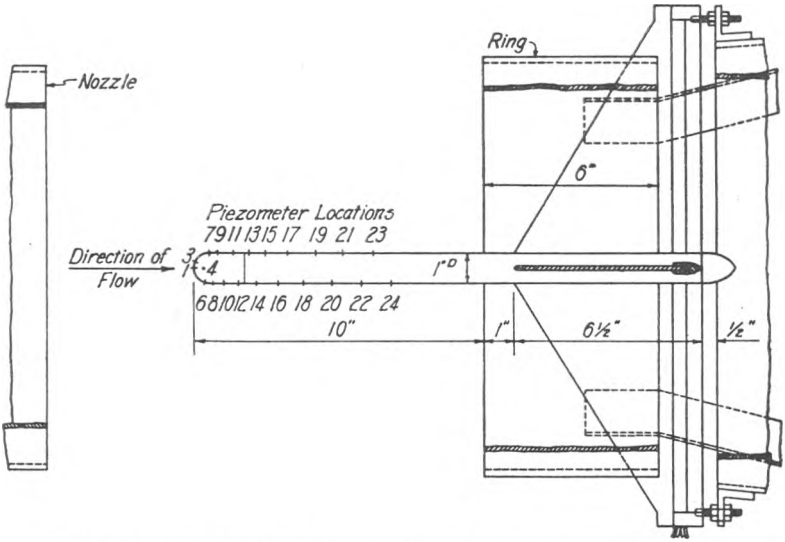

FIG. 4. DETAILS OF SHAFT AND MOUNTING FOR THE VARIOUS HEADS.

section. Along the top and bottom of the shaft are 12 $\frac{1}{32}$-inch piezometers, and in the end are 12 additional holes matching the piezometer leads in the interchangeable heads. Copper-tubing leads were carried through the shaft nearly to the rear, passing through slots in the shaft wall to form the leading edges of the streamlined cross struts.

The various heads may be secured to the shaft by means of a threaded stainless-steel rod, a streamlined knob at the downstream end permitting the head to be firmly seated. The 12 piezometer openings in each head are arranged in four longitudinal rows which can be brought to a position at the top or bottom or either side as the head is turned (see Fig. 5). Leads from these piezometers pass

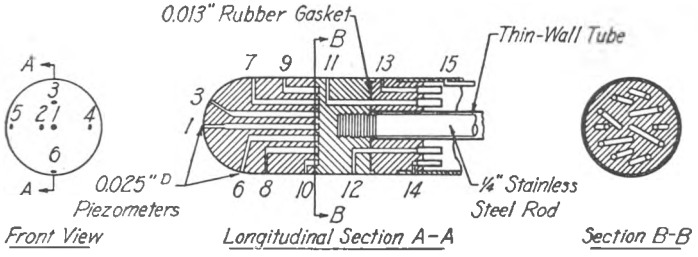

FIG. 5. VERTICAL SECTIONS THROUGH A TYPICAL HEAD.

to holes in the base which match those at the end of the shaft when the head is in any one of the four positions. A thin rubber gasket punched to match the piezometer leads prevents leakage across the joint when the head is tightly secured. Two small pins serve to align gasket and head in each of the four optional positions. All external surfaces are nickel plated.

As a check on the agreement between the finished heads and the specified forms, a number of the heads were checked with a toolmaker's microscope, some at the Rock Island Arsenal and others at the Taylor Model Basin. These checks indicated a high degree of accuracy in the machining process, discrepancies being for the most part less than 0.001 inch, and never over 0.003 inch.

The 24 piezometer leads from the test shaft pass through the wall of the test section to a petcock manifold, which is immersed in a water bath to avoid leaks when under vacuum. A master lead from this manifold and a lead for the piezometer plate in the wall of the test section are connected to a third differential mercury manometer. This manometer (see Fig. 1) is so arranged as to permit differential heads to be read by vernier to 0.001 foot over a maximum range of 4 feet; it is of a convenient zero-displacement design, a mercury pot and graduated rod being raised or lowered by rack and pinion until the mercury level in the opposite leg of the flexible U-tube is brought to a fixed mark in a stationary glass tube. Pendulation of the mercury column is held to a practicable minimum by means of fine glass capillary bypasses in the piezometer leads.

In order to make supplementary studies comparing flow in open and closed throats, a cylindrical brass shell was constructed in such a manner that it could be installed in the open-throat test section. In this way the same test mounting could be used and easy interchangeability was achieved. Made of $\frac{1}{8}$-inch brass plate, the shell is 24 inches long and of the same inside diameter (about 13 inches) as the nozzle. With a removable cover it served to confine the jet throughout the test section, at the same time permitting ready access to the models. Although the junctions at the nozzle and around the cover were reasonably tight, no attempt was made to close the gap between the enclosure and the tunnel at the downstream end of the test section.

III. PRELIMINARY INVESTIGATIONS

As a necessary part of the cavitation studies described herein, preliminary measurements were made for purposes of calibration and for the determination of certain practical limitations of the equipment. That is, information was sought concerning the degree of uniformity of flow in the test section, the calibration of the pressure and velocity gages, the extent of viscous influences, the effect of relative model size, and the degree to which cavitation studies would be influenced by the release of air from solution. In addition a comparison was desired between characteristics of flow around the same bodies in open and closed throats.

The variation of pressure in the test section along the axis of the jet was determined with a 1-inch-diameter brass tube considerably longer than the test section, and having eight $\frac{1}{32}$-inch holes drilled around a normal section at about mid-length. The tube was adjustable in the longitudinal direction, thus permitting the piezometer openings to be placed at any point along the centerline of the jet. The pressures determined in this manner were referred to piezometers either in the side of the test section or in the lip of the nozzle. In addition, both velocity-head and piezometric-head traverses across the jet were made with a Prandtl-type Pitot tube. The latter tube was $\frac{3}{8}$-inch in diameter and 6 inches long, and was mounted on a 1 x $\frac{3}{8}$-inch shaft extending through the jet on both sides of the tube to avoid asymmetry.

Since small but systematic spatial variations in piezometric head (i.e., $h = p/\gamma + z$) were thus disclosed, an arbitrary reference point was required, and the region of primary interest — i.e., immediately upstream from the point at which the models were attached to the shaft — was selected. Further differences, of the order of 1% of the velocity head, were found between the piezometric heads determined by the longitudinal shaft and by the side openings of the Pitot tube; these differences were not identical for the open and the closed throats. Comparisons were made with the measured distributions of piezometric head around a hemispherical profile, followed by repeated careful observations under various conditions of flow and by simultaneous measurements with both techniques. As a result, slight corrections were established to bring the data into essential agreement. Specifically, the indications of the Pitot static openings were found to be slightly over a percent high because of the obstruction of the supporting rod, and corrected accordingly;

in addition, an arbitrary adjustment of less than a percent was made to bring the results of the two types of measurements into substantial agreement as shown in Fig. 6. The radial scale and the longitudinal position of the model are indicated by the inserted drawing of the 1-inch hemispherical head. It should be noted that the dimensionless pressure scale is exaggerated, being five times

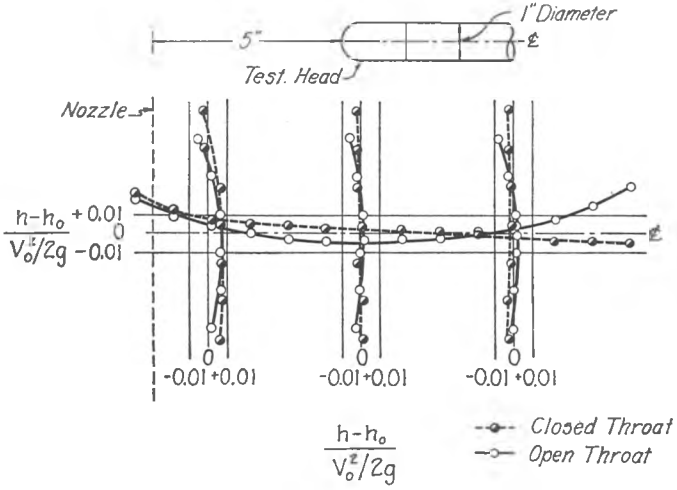

FIG. 6. DISTRIBUTION OF PIEZOMETRIC HEAD IN CLOSED AND OPEN THROATS.

that used in presenting the results from the studies of the various head forms.

The velocity traverses for the closed throat evidence a remarkably uniform velocity distribution in the region of primary interest, while the jet in the open throat is seen to be incompletely formed (see Fig. 7). Good agreement is indicated by the tendency for the velocity head and piezometric head to vary in opposite directions from their mean values. Both types of traverse point to the presence of a slight asymmetry of flow in the vicinity of the nozzle. The existence of this anomaly was also indicated by a series of readings taken for the purpose of aligning the test shaft with the flow. Measurements were made with a 1-inch hemispherical head oriented successively in each of the four possible positions, and the inclination of the shaft was then adjusted both horizontally and vertically until each piezometer yielded the same head readings in all positions. In this manner the open-throat jet was found to have a

downward inclination of a little more than 2°. Although exploratory tests indicated a rather pronounced non-uniformity of velocity in the approach section, partial screening of the louvers and the insertion of a honeycomb did not substantially improve the condition. Further measures were not taken because it was felt that the non-uniformity in the test section, while undesirable, was small.

Both the pressure and the velocity gages were calibrated from the traverses shown in Figs. 6 and 7, taking as the point of reference the same central region already mentioned. The piezometer plate in the side of the test section and the single piezometer in the lip of the nozzle were found to require slight corrections which were proportional to the velocity head of the jet, and differed somewhat for the open and closed throats.

Although the distribution of piezometric head around a submerged body is a function of the Reynolds number $\mathbf{R} = V_0 d/\nu$, at

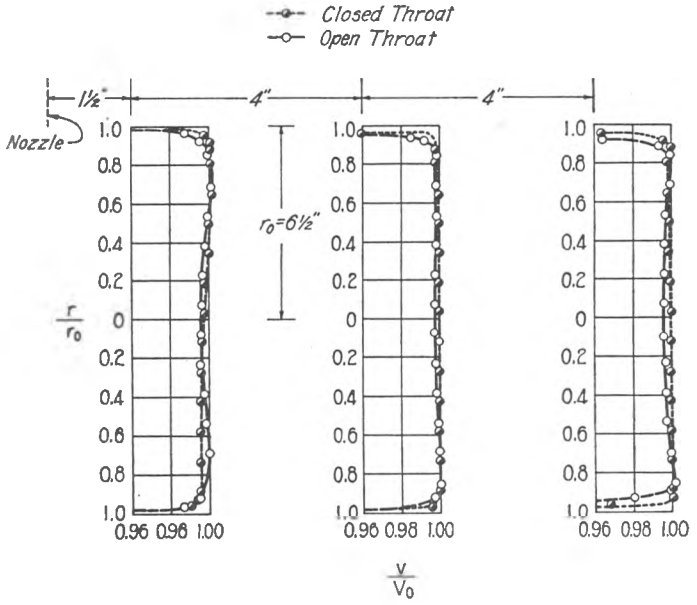

FIG. 7. VELOCITY DISTRIBUTION IN CLOSED AND OPEN THROATS.

moderately high values of this parameter the boundary layer becomes turbulent, the pattern of flow becomes stable, and further increases in **R** produce no further change in pressure distribution. As a preliminary to determining the effect of cavitation upon the pressure distribution for each form, therefore, a series of runs were

made at atmospheric pressure for different Reynolds numbers. The results of such a test on the hemispherical head form are shown in Fig. 8. (Herein, as is also true of subsequent diagrams, the change in piezometric head in its ratio to the velocity head of the undisturbed flow is plotted against the ratio of the distance along the boundary to the head diameter.) This plot indicates for the hemispherical head an approximate critical value of $\mathbf{R} = 2\text{x}10^5$; a

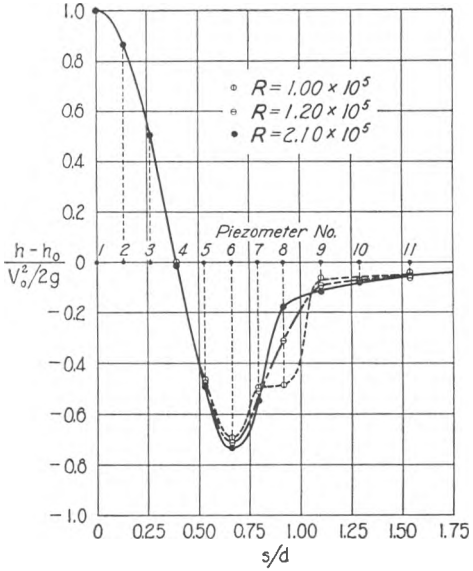

FIG. 8. VARIATION IN PRESSURE DISTRIBUTION WITH REYNOLDS NUMBER FOR HEMISPHERICAL HEAD.

threefold increase above this critical produced no further change in the pressure distribution. Because it was understood that the experiments described herein would be utilized for prototype design in the high Reynolds-number range, a critical value of **R** was determined for each head form (except for three beyond the capacity of the tunnel) and all subsequent tests were made at a higher value.

The magnitude of this upper critical Reynolds number varies considerably with the head form, being greatest for boundaries of moderate length. The pressure distributions for three of the forms tested — the $\frac{1}{8}$-caliber rounded, the 45° conical, and the $\frac{1}{2}$:1 ellipsoidal — continued to vary with the Reynolds number throughout

the entire range of the tunnel. Furthermore, the flow past the two rounded forms was found to be unstable, as it tended alternately to follow the irrotational pattern and to form a small but definite pocket of separation. Both the shorter and the longer forms became stable within or below the range of the tunnel, but for quite different reasons. Flow past blunt and concave forms achieves a stable separation pattern beginning at the abrupt change in boundary, while on longer forms the separation either does not occur or is eliminated by turbulence at comparatively low values of **R**. For the unstable intermediate forms, as **R** increases the separation is reduced and the value of the minimum pressure is also reduced; a limiting value is achieved, but only at higher values of **R**.

To determine the degree to which flow conditions in the closed and open throats differed from those for an infinite fluid stream, an additional study was made of the effect of relative model size by measuring the pressure distributions around a series of bodies 1, $1\frac{1}{2}$, 2, 3, and 4 inches in diameter. As shape was not considered an important variable, and as the hemispherical head form was thought to be the most representative of the several series, only this one form was studied. The various models were made in such a manner that they could be mounted on the 1-inch test shaft, the parallel afterbody being carried well to the rear of the test section. To simplify construction, only the more significant region indicated by holes 1-12 was investigated. (Although the head forms and hole locations were apparently similar in every respect, it was to be expected that non-uniformities of flow throughout the jet and slight variations in the finished models would introduce additional small variations. In the latter connection it is to be noted that a measurable difference in the minimum pressure for two different 1-inch hemispherical heads was found, although microscopic comparison showed the two to differ in contour by a maximum of only 0.003 inch.)

Pressure distributions around the various heads for flow without cavitation are presented in dimensionless form in Figs. 9 and 10 for the closed and open throats, respectively. (It is to be noted that the quantity $(h - h_0)/(V_0^2/2g)$ becomes closely indicative of $(p - p_0)/(\varrho V_0^2/2)$ as h_0 becomes large compared with d — i.e., as the effect of small changes in elevation becomes negligible. The distribution of pressure is therefore considered synonymous with that of the measured piezometric head through the remainder of the

paper.) The significant feature of the plots is the contrast between the systematic downward shift of the curves with increasing head size for the closed throat and the relatively slight displacement of the results for the open throat. In this connection it should be pointed out that, although the various head forms were not tested at the same Reynolds number because of the considerable differences in diameter, all tests were performed at values of **R** above the critical. Furthermore, measurements were made for several different values of **R** and no variation was found. Hence the systematic displacement of the curves in Fig. 9 is not the result of viscous

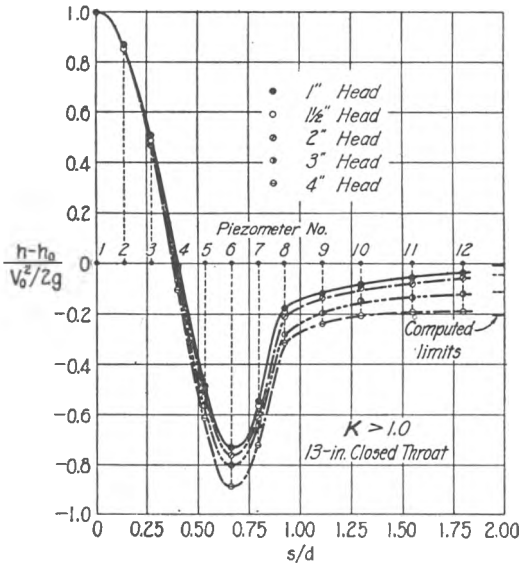

FIG. 9. VARIATION IN PRESSURE DISTRIBUTION WITH MODEL SIZE IN CLOSED THROAT.

effects. On the contrary, the spread is directly related to the decrease in cross-sectional area of flow, the horizontal lines at the right of the figure indicating the asymptotic values computed from the mean increases of velocity produced by the constriction, application of the Bernoulli equation leading to the approximate relationship $(h - h_0)/(V_0^2/2g) = 2(d/D)^2$ for small values of d/D. On the other hand, the absence of any appreciable difference in the distributions for the open throat — even for the case in which the area of the obstruction was approximately 10% of the original jet area — indicates a divergence of the outer boundary of the jet in

place of an increase in jet velocity. Such divergence is facilitated by the fact that the receiving ring and tunnel conduit downstream from the test section have a diameter nearly 15% larger than that of the nozzle.

Similar measurements made at various intensities of cavitation gave indications similar to those for flow without cavitation. Because of the lower local pressures around the larger heads in the closed throat, cavitation began at relatively higher centerline pressures, and was more intense at any given pressure than for the smaller heads. Variation of head diameter in the open throat again

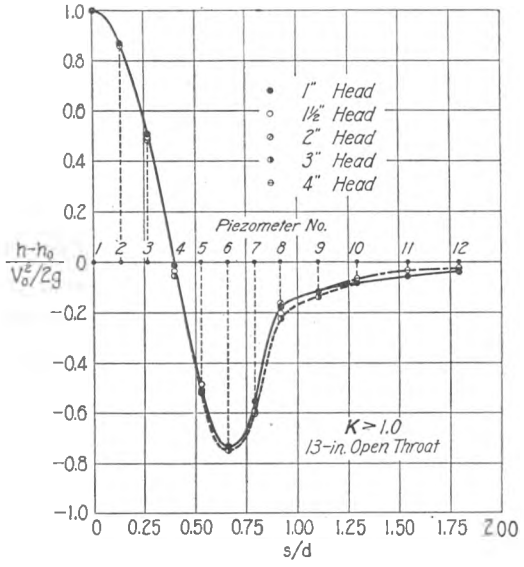

FIG. 10. VARIATION IN PRESSURE DISTRIBUTION WITH MODEL SIZE IN OPEN THROAT.

produced no effects of significance throughout the range of practical interest. Hence, while it was found that use of an enclosed jet insures greater uniformity in the distribution of velocity and pressure in the undisturbed flow, use of an open throat permits the investigation of proportionately larger models without appreciable distortion of the pressure distribution even under conditions of severe cavitation.

The final series of preliminary tests dealt with the influence of air content upon the cavitation phenomenon. If the vapor pressure of the water is expressed in terms of the corresponding head h_v, and

and the partial pressure of air liberated from solution by h_a, the ratio $(h_0 - h_v - h_a)/(V_0^2/2g)$ should be the primary criterion for the cavitation characteristics of a given body profile. The effect of any dissolved gas is to decrease the magnitude of the numerator of this cavitation index. Since the water supplied to the present tunnel contains a considerable amount of air in solution, short periods of de-aeration (i.e., operation at low pressure for an hour or more) are necessary to reduce this amount to a practicable minimum. Although no instrument for measuring the air content of the water has been installed, the experiments show that pressure measurements made under heads less than 0.5 foot of water above the de-aeration pressure are distorted by air coming out of solution, while at somewhat higher pressures (and correspondingly higher velocities) no measurable distortion of the results is found. Consequently, the technical difficulties in evaluating h_a may be avoided by keeping the air content low and by maintaining a pressure head at least 0.5 foot of water above the de-aeration pressure. That dissolved air should in general have no appreciable effect upon cavitation phenomena under field conditions is evident from the fact that h_0 is then almost invariably high (usually greater than the atmospheric pressure head). Hence the quantity h_a will be disregarded in the remainder of this paper.

IV. Effect of Cavitation Upon the Distribution of Pressure Around Bodies of Revolution

For flow past submerged bodies at high Reynolds numbers, the distribution of pressure is a function of the boundary geometry and degree of cavitation [1], the extent of cavitation effects being defined by a dimensionless number which has been designated as **K**. Although several definitions are possible, for flow past a submerged body **K** is usually expressed in the form

$$\mathbf{K} = \frac{h_0 - h_v}{V_0^2/2g}$$

The numerator evidently is a measure of the maximum drop in pressure which can occur at any point, and the denominator is a reference parameter based upon the maximum possible pressure rise — i.e., at a point of stagnation. An increase in the numerator or a decrease in the denominator of this fraction thus represents a reduction in the tendency toward cavitation. Low values of **K** are therefore associated with high cavitation tendencies.

Since over most of the practicable range of hydraulic phenomena the flow is entirely independent of vaporization effects, only in the event that a local pressure decreases to the vapor pressure of the liquid does a further reduction of the cavitation parameter produce any significant effect. It is thus expedient to define $\mathbf{K}_i$ as that value of $\mathbf{K}$ at which cavitation is incipient, all values of $\mathbf{K}$ greater than $\mathbf{K}_i$ therefore yielding a pattern of flow unaffected by cavitation. As $\mathbf{K}$ is reduced below this critical value, however, the effects of cavitation become more and more pronounced, the extent of the effect being indicated by the relative magnitudes of $\mathbf{K}$ and $\mathbf{K}_i$. This trend is demonstrated by the systematic variations in pressure distribution for flow past hemispherical and blunt head forms shown in Figs. 11 and 12, respectively.

Each of these figures includes at the top a half section through the body in question, indicating the general relationship between the pressure-distribution curve (plotted normal to the boundary) and the body profile. This same curve is plotted against developed distance along the profile in the graph below. For $\mathbf{K} > \mathbf{K}_i$ all distribution measurements were found to coincide very closely. For values of $\mathbf{K}$ less than $\mathbf{K}_i$, on the other hand, a systematic variation in each series of distribution curves will be readily apparent. As $\mathbf{K}$ decreases, in other words, the formation of a cavitation pocket (shown in silhouette in the photographs of Figs. 13 and 14) results in a proportionate lengthening of the zone of minimum pressure, and at the same time a reduction in the relative magnitude of the pressure drop. That the rather abrupt end of the minimum-pressure zone is a continuous function of $\mathbf{K}$ may be seen from the upper curve in each diagram. Comparison of this curve with the pocket silhouettes (presented in detail in the Appendix) will indicate that the end of the pocket invariably lies a short distance downstream therefrom, just prior to the point of full pressure recovery.

The variation of the minimum pressure with $\mathbf{K}$ is shown at the right of each figure. Such curves may safely be extrapolated to zero, since for small values they necessarily coincide with a 45° line passing through the origin (i.e., h_{min} must approach h_v as a limit). Although having comparable asymptotes, the specific minimum-pressure curves for these two head forms differ widely, since they typify the two types of stable flow described in Section III. In flow past the blunt head a stable separation pocket occurs, and cavitation actually begins in the fine-scale eddies along the surface

of discontinuity immediately beyond the point of minimum pressure. As a result, cavitation effects first occur when the minimum pressure on the boundary is still well above vapor pressure; only for very low values of the cavitation number ($\mathbf{K} < 0.3$) does the minimum boundary pressure approach the vapor pressure. In contrast with this, the corresponding curve for the hemispherical form approaches as a theoretical limit the linear asymptotes, the minimum pressure occurring near the boundary in the absence of an appreciable zone of separation.

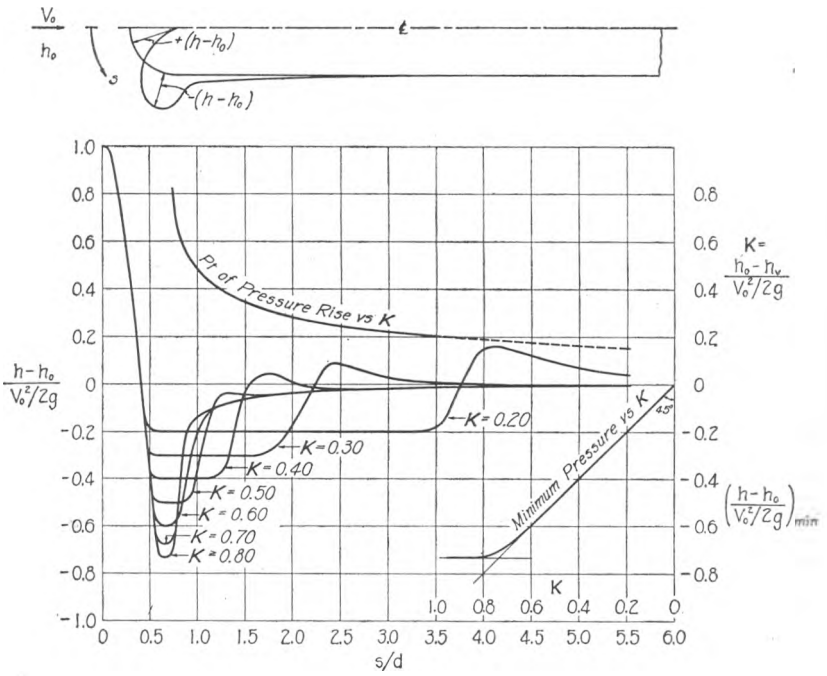

FIG. 11. EFFECT OF CAVITATION UPON THE PRESSURE DISTRIBUTION AROUND A CYLINDRICAL BODY WITH HEMISPHERICAL HEAD.

In order to provide as complete information as possible from tests on a limited number of models, three systematic series were selected and varied from long through intermediate to blunt and concave forms, as shown in Fig. 15. Rounded, conical, and ellipsoidal shapes were chosen, in order that the test results could be adapted to a wide variety of forms either directly or by interpolation. Since each of the heads within a series may be characterized by a single length ratio, the individual pressure distributions repre-

sent one of the family of curves defined by the functional relationship

$$\frac{h - h_0}{V_0^2/2g} = f\left(\text{type}, \frac{a}{b}, \mathbf{K}\right)$$

where "type" refers to the general classification (e.g., rounded) and a/b becomes r/d for the rounded series, l/d for the conical, and the axis ratio for the ellipsoidal. For obvious reasons the hem-

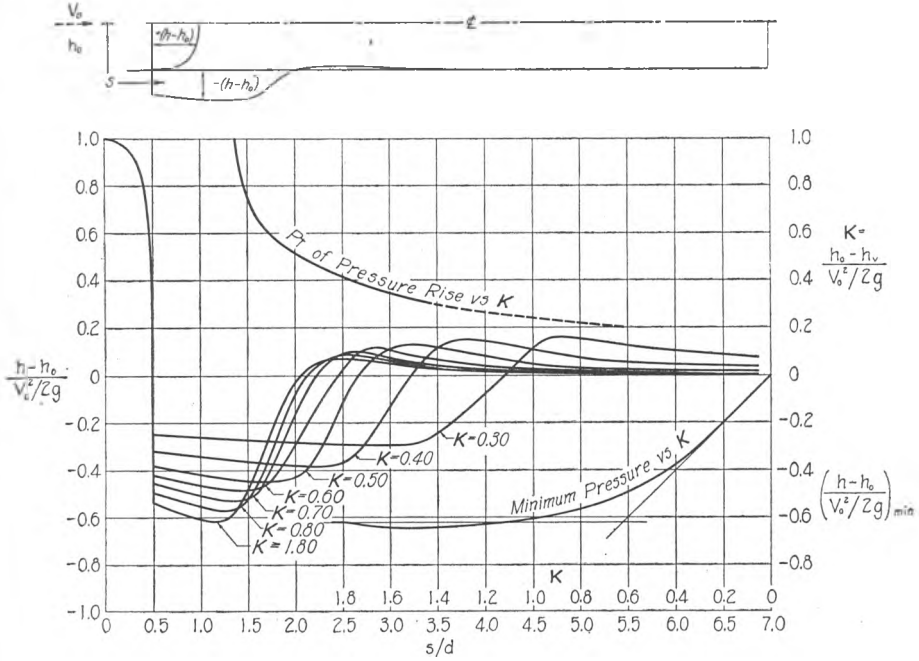

FIG. 12. EFFECT OF CAVITATION UPON THE PRESSURE DISTRIBUTION AROUND A CYLINDRICAL BODY WITH BLUNT HEAD.

ispherical and the hollow cylindrical forms appear in two and the blunt in three of the different series.

Individual reports for each of the head forms — including plots similar to Figs. 8 and 11, silhouette photographs, and tabulated data — have been prepared for limited circulation by the Bureau of Ships, U. S. Navy. Since the primary purpose of this bulletin is to provide general information for a variety of boundary conditions, the emphasis herein will be placed upon the analysis and summarization of the results, rather than the presentation of a large number of data and curves. However, plots of pressure distribution

and pocket profile for each of the heads are included in the Appendix.

Rounded Series

The first series consisted of forms in which the basis of the profile was the circular arc. For descriptive purposes, the caliber of rounding has been defined as the ratio of the radius of curvature of the head profile to the shaft diameter. It may be seen from Fig. 15, therefore, that calibers of 0, $\frac{1}{8}$, $\frac{1}{4}$, $\frac{1}{2}$, 1, and 2 were included in this series. Fig. 16 represents the orderly sequence of pressure-

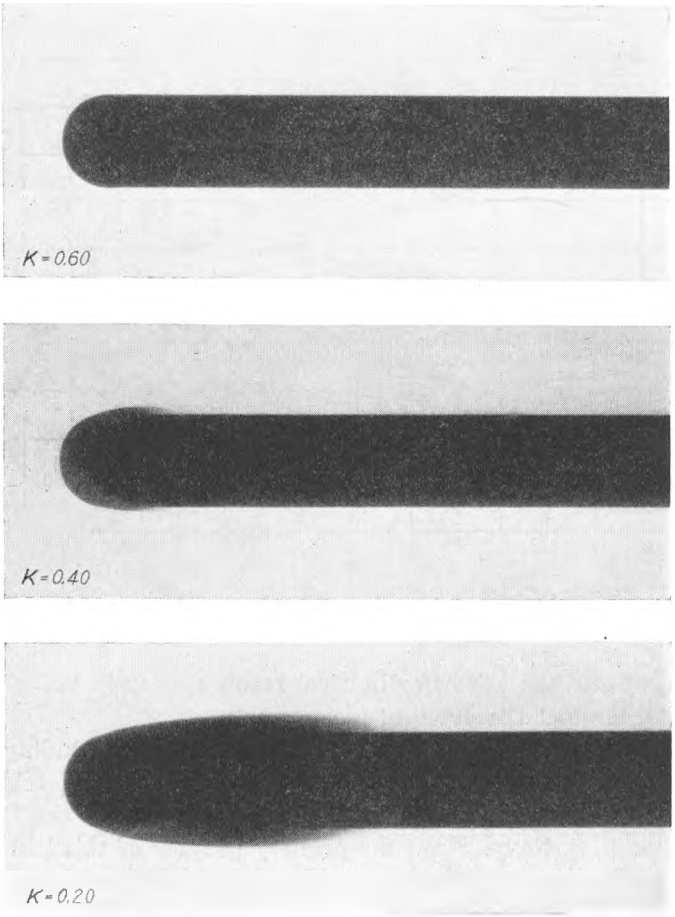

FIG. 13. SILHOUETTES OF VAPOR POCKET FORMED BY A HEMISPHERICAL HEAD AT VARIOUS MAGNITUDES OF THE CAVITATION INDEX.

distribution curves for this family of head forms under conditions free from cavitation and for sufficiently high Reynolds numbers to assure a stable flow pattern. The abscissa scale is the relative longitudinal distance from the juncture of the head curve with the uniform afterbody.

While these graphs are based upon measurements, slight experimental inconsistencies have been eliminated by the method of adjusting intercept values along horizontal and vertical lines to yield smooth curves when plotted against head caliber. Since this method

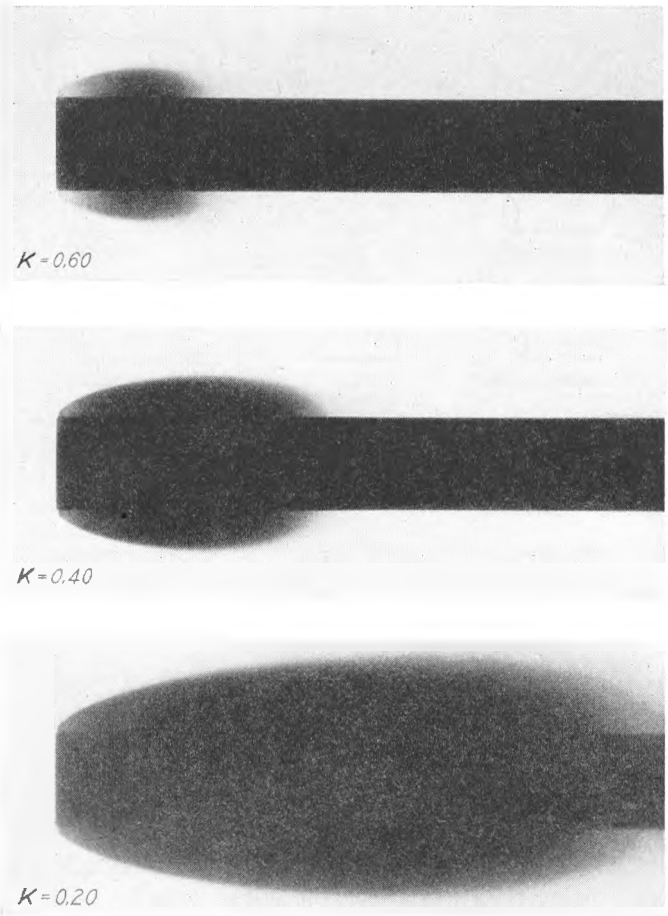

FIG. 14. SILHOUETTES OF VAPOR POCKET FORMED BY A BLUNT HEAD AT VARIOUS MAGNITUDES OF THE CAVITATION INDEX.

also yields directly the coordinates of the pressure curve for any intermediate caliber, curves have been included for other calibers than those tested. While the extrapolated curves for the 3-caliber ogival head, as well as those for most of the intermediate calibers, are considered to be reasonably accurate, note must be made of the

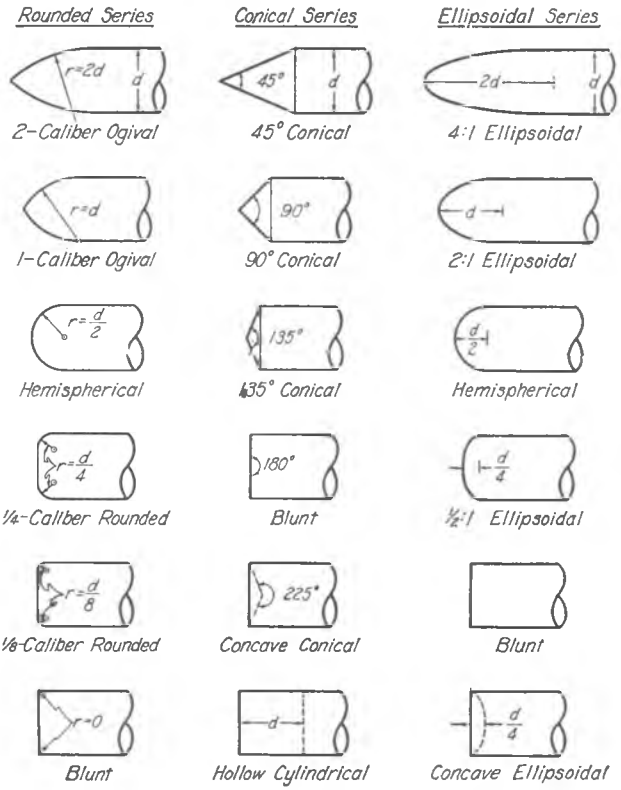

FIG. 15. HEAD FORMS STUDIED IN THE ROUNDED, CONICAL, AND ELLIPSOIDAL SERIES.

fact that the $\frac{3}{16}$-caliber and the $\frac{1}{16}$-caliber curves involve a certain amount of estimation. This is due in part to the instability of flow around the short-radius forms, and in part to the arbitrary adjustment of the $\frac{1}{8}$-caliber measurements to approximate a higher Reynolds number than was attainable in the tunnel.

For want of more explicit information it is sometimes necessary to estimate the magnitude of **K** for incipient cavitation from the minimum value of $(h - h_0)/(V_0^2/2g)$ on a plot such as that of

Fig. 16. This is tantamount to assuming that during cavitation the magnitude of the cavitation index will agree numerically with the minimum value of the pressure parameter on the distribution curve — i.e., that $\mathbf{K} \approx \left(\frac{h - h_0}{V_0^2/2g} \right)_{min}$. As will be seen from Fig. 17, nevertheless, displacement of the lowest point of the pressure-distribution curve invariably begins at a higher value of **K** than would be indicated by the foregoing assumption. In the case of the blunt head form, the cavitation in the fine-scale eddies along the surface of separation results in a change in flow pattern which at first even tends to lower the pressure intensity at the boundary itself. As may be observed from the sequence of curves in Fig. 17, the gradual asymptotic approach of each to the 45° line representing the assumed function would indicate that similar conditions of incipient cavitation prevail for even the larger-caliber heads; in other words, separation — or at least the formation of additional boundary eddies — appears to produce local pressure intensities within the flow which are lower than that at the boundary and hence first attain the vapor-pressure magnitude. While the intersections of the 45° line with the horizontal asymptotes of the several curves represent the values of $\mathbf{K}_i$ which would be predicted from the pressure distribution, the larger values indicated by the initial displacement of the pressure-distribution curves are considered more nearly representative of actual conditions of incipient cavitation.

These two series of values are plotted against caliber of rounding in Fig. 18, for purposes of further comparison. In order to attain the zero point on the caliber scale, an arithmetic progression is used in the graph at the left, while a logarithmic plot is used at the right to permit extrapolation with greater accuracy. It is apparent from the former that minimum-pressure conditions are to be expected between $\frac{1}{8}$ and $\frac{3}{16}$ caliber of rounding — the $\frac{1}{8}$-caliber head, in fact, yielding very unstable flow conditions. Beyond this point the two curves approach one another very slowly, at the same time gradually decreasing in slope, corresponding in the logarithmic plot to parallel straight lines. The solid points and the broken curve in the graph at the right represent results obtained by visual determination of initial vapor-pocket formation in the water tunnel at the California Institute of Technology [2].

As already mentioned with regard to the blunt and hemispherical heads, during cavitation the pressure intensity along all heads of this series is essentially constant over almost the entire length of

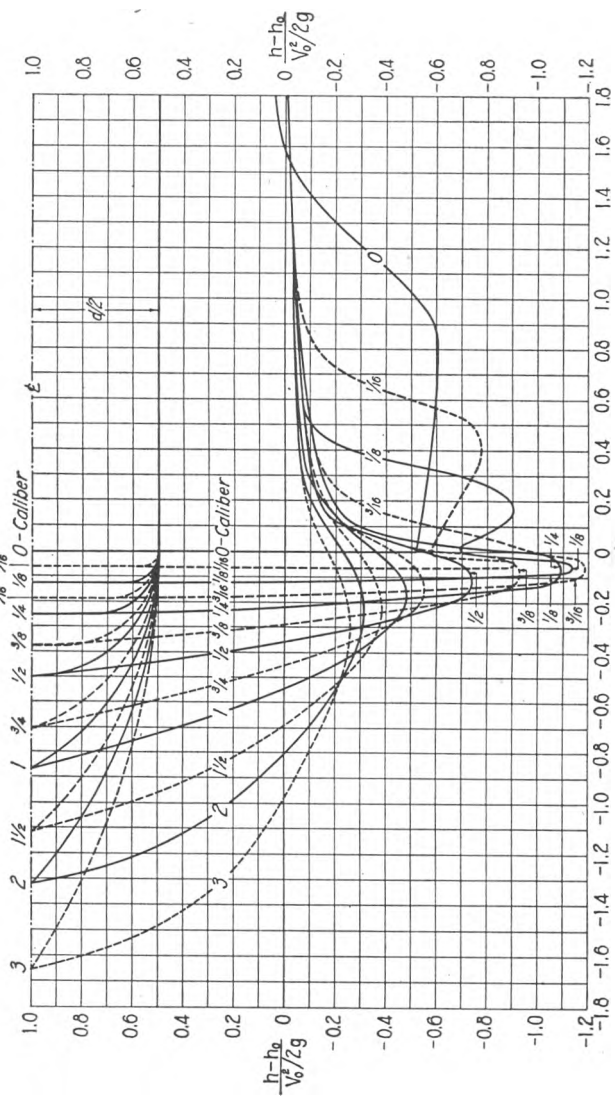

FIG. 16. LONGITUDINAL DISTRIBUTION OF PRESSURE FOR THE ROUNDED SERIES AS A FUNCTION OF CALIBER OF ROUNDING.

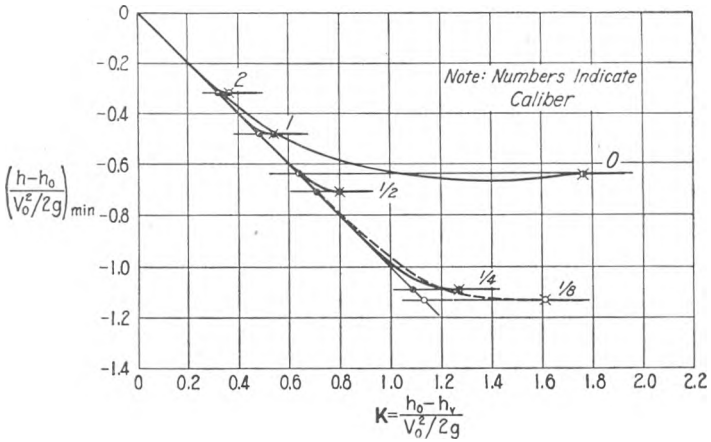

FIG. 17. VARIATION OF MINIMUM PRESSURE WITH CAVITATION NUMBER FOR ROUNDED HEAD FORMS.

the visible vapor pocket. Careful comparison of the pocket silhouettes with the pressure-distribution curves (refer for both to the Appendix) indicated that (except for early stages with the blunter forms) the beginning of the pocket invariably coincided with the drop in pressure, whereas the end in each case occurred at approximately the midpoint of the curve of pressure recovery. In other words, although the individual vapor bubbles form as the pressure approaches p_v, they do not collapse until they have been carried an appreciable distance into the zone of increasing pressure. It is

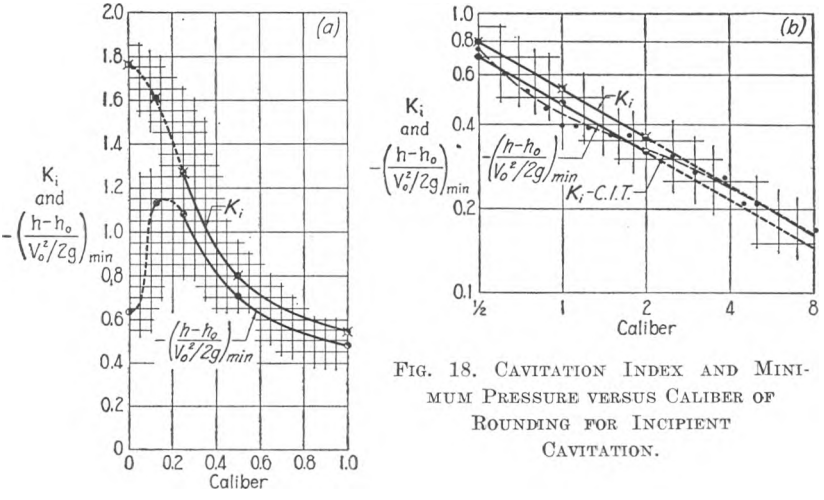

FIG. 18. CAVITATION INDEX AND MINIMUM PRESSURE VERSUS CALIBER OF ROUNDING FOR INCIPIENT CAVITATION.

to be noted, of course, that time photographs of the type used in this study do not reveal the instantaneous details of the formation and collapse cycle [3]. On the other hand, plots of the point of pressure rise, end of visible pocket, and maximum pocket diameter against the cavitation index for each head form verify the systematic trend of the series of silhouettes reproduced in the Appendix, and hence are most representative of the mean conditions discussed herein.

At the edges of the blunter heads, it will be noted (see Figs. 51-53), the outline of the mean vapor pocket does not begin at the corner of the head profile, as would the normally assumed surface of separation, but somewhat farther downstream. In seeking an explanation of this phenomenon, it must be recalled first of all that the separation pattern is controlled not only by the shape of the front face, but also by the presence of the parallel afterbody, which tends to decrease the size and increase the intensity of the eddy enclosed by the separation surface. At the upstream end of this eddy, curvature of the stream lines of the reverse flow must necessarily reduce the local cavitation tendency. Along the separation surface, moreover, it cannot be expected that the fine-scale vortices, and the accompanying cavitation at their cores, would develop immediately even in a fluid so slightly viscous as water. Although for these reasons the pocket silhouette might be expected to advance upstream to the corner of the head as the pocket became completely filled with vapor at very low values of **K**, a slight capillary creep could still result in some overhang. That the silhouette does appear to begin at the corner of the concave heads is probably an optical effect, since the outline of the entire three-dimensional pocket rather than that of the desired longitudinal section necessarily resulted from the photographic technique in use.

Conical Series

The second series consisted of right circular cones mounted on the parallel afterbody, apex angles of 45°, 90°, 135°, 180°, 225°, and 360° being selected as representative forms. In the preparation of the final plots, however, it was found desirable to construct and test two additional forms with apex angles of $22\frac{1}{2}°$ and $67\frac{1}{2}°$.

As an aid in systematizing the results, considerable attention was given to a mathematical analysis of flow with comparable boundary conditions. Although no method was found which would yield the

theoretical pressure distribution for the conical surfaces studied, sufficient similarity was found between the experimental results and the theoretical distribution for two-dimensional cones (or wedges) to justify a detailed analysis of the latter type of fluid motion.

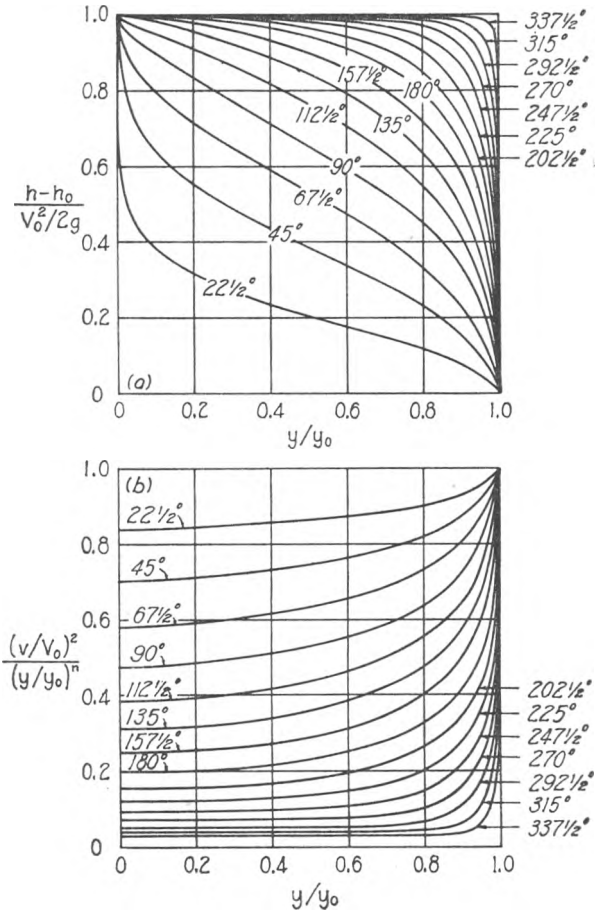

FIG. 19. CHARACTERISTIC CURVES FOR FLOW WITH SEPARATION PAST TWO-DIMENSIONAL CONES.

From the equations presented by Lamb [4] for symmetrical flow with separation past a bent lamina, a conformal solution for the two-dimensional cone was completed. The resulting relationship between the ratios y/y_0 and v/V_0 is expressible by means of an infinite series in the form

$$\frac{y}{y_0} = \frac{2}{J}\left(\frac{v}{V_0}\right)^{\frac{2-\varphi}{\varphi}} \sum_{s=1}^{\infty} \frac{(2s)^2}{2s-\varphi}\left(\frac{v}{V_0}\right)^{\frac{2(s-1)}{\varphi}}$$

where y and y_o are, respectively, the lateral distances to a general point on the lamina and to the point of separation, and J is a function of φ, the ratio of the apex angle to π:

$$J = 1 + \varphi + \frac{\varphi^2}{2}\left[\frac{8}{(4-\varphi)(2-\varphi)} + F\left(\frac{4-\varphi}{4}\right) - F\left(\frac{2-\varphi}{4}\right)\right]$$

The F-function, $F(a) = \int_0^1 \left(-\frac{1}{\ln a} - \frac{z^a}{1-z}\right) dz$, was tabulated by Gauss [5]. The family of curves in Fig. 19(a), in which the pressure-distribution parameter is plotted against the geometric ratio y/y_0, was computed from the foregoing equations.

Since the summation may be represented by the first term of the series for small values of v/V_0, the equation may be written in the approximate but significant form

$$\frac{(v/V_0)^2}{(y/y_0)^n} = \left[\frac{(2-\varphi)J}{8}\right]^n$$

where $n = 2\varphi/(2-\varphi)$. The right-hand term is evidently a constant for a given apex angle, and represents the limiting value of

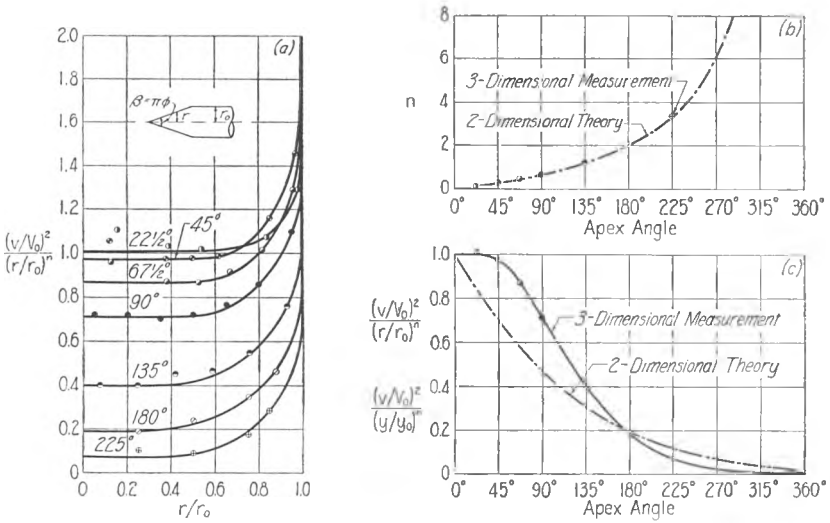

FIG. 20. COMPARISON OF MEASUREMENTS FOR THREE-DIMENSIONAL CONES WITH THEORETICAL RESULTS FOR TWO-DIMENSIONAL CONES.

the ratio $(v/V_0)^2/(y/y_0)^n$ at the tip. In fact, as may be seen from the plot of the data with $(v/V_0)^2/(y/y_0)^n$ as ordinates in Fig. 19(b), the approximate relationship closely represents the exact equation over a radial distance which increases rapidly with increasing apex angle.

In order to utilize the similarity between theory and experiment, Fig. 20(a) was prepared in the same manner as Fig. 19(b). The exponents used for both plots, and the limiting constants which were obtained, are shown in Figs. 20(b) and 20(c). Although the coefficients follow a somewhat different functional trend, it is noteworthy that the assumption of equal exponents for the two- and three-dimensional systems appears to be entirely justified by the experimental data, and the analytical results were therefore of considerable aid in the preparation of the generalized experimental plots.

Fig. 21, containing the sequence of pressure-distribution curves for conical head forms, is comparable to Fig. 16 for the rounded series, the curves representing the pressure distributions in cavitation-free flow at high Reynolds numbers. As before, the experimental curves were adjusted slightly and interpolated values were included. Although the results for the 45° cone varied with the Reynolds number throughout the range of the water tunnel, this variation was not pronounced for the higher Reynolds numbers; the interpolated values are therefore considered to be reasonably accurate throughout. The curve for the apex angle of 360° has been moved slightly to the right in Fig. 21, because the initial inside diameter of the hollow cylindrical head was actually 2% less than the outside diameter and its walls had a combined taper of 5°.

Although it was assumed in the mathematical analysis of such head forms that the presence of the parallel afterbody had no effect upon the geometry of the separation zone, it will be found from an examination of Fig. 21 that the afterbody influence is actually quite appreciable. For example, the lowest pressure at the trailing edge of a cone without afterbody should be obtained with the maximum apex angle of 360°, whereas with afterbody the pressure in this region is a minimum for an angle of approximately 45°, increasing steadily therefrom as the head becomes either sharper or blunter. The cylindrical afterbody, in other words, tends to decrease the separation tendency to at least some degree in all

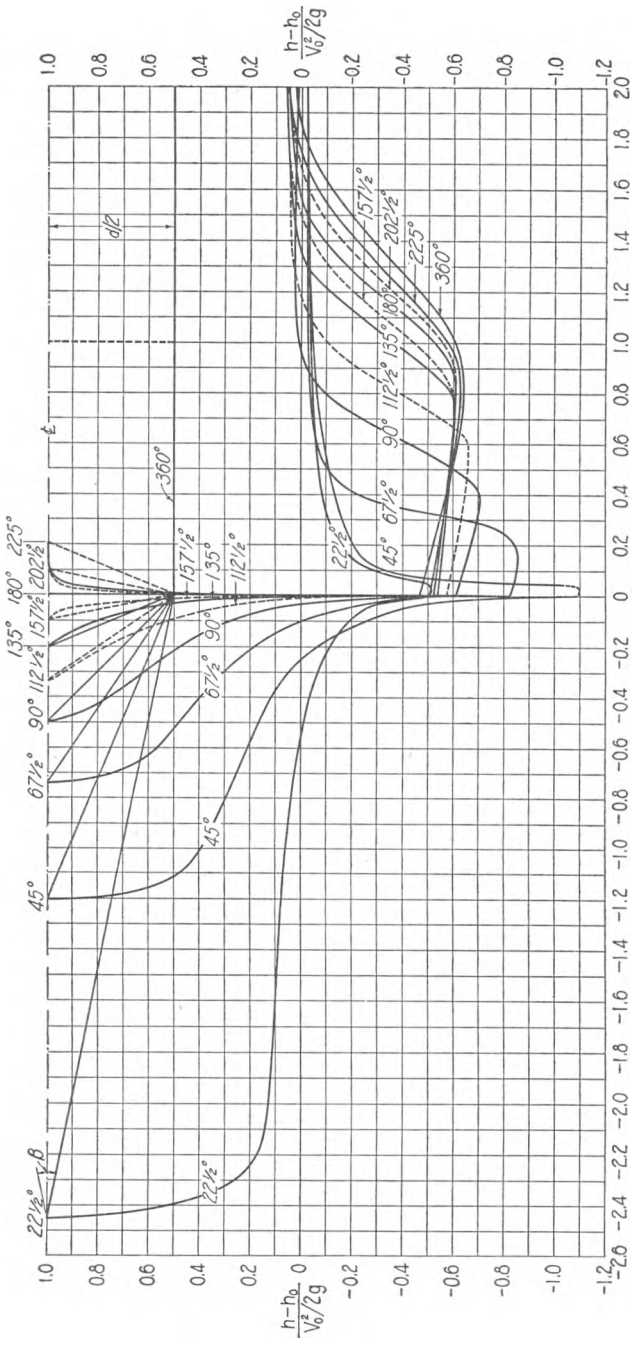

FIG. 21. LONGITUDINAL DISTRIBUTION OF PRESSURE FOR THE CONICAL SERIES AS A FUNCTION OF THE APEX ANGLE.

cases, with the result that the approximation to irrotational conditions without separation in the case of small to moderate apex angles yields the lowest boundary pressures for these heads. The afterbody will be found to have a similar effect upon the separation tendency in both the rounded and the ellipsoidal series.

Particularly noteworthy in the plots of the minimum pressure-head ratio versus **K** for the conical series (Fig. 22) is the pro-

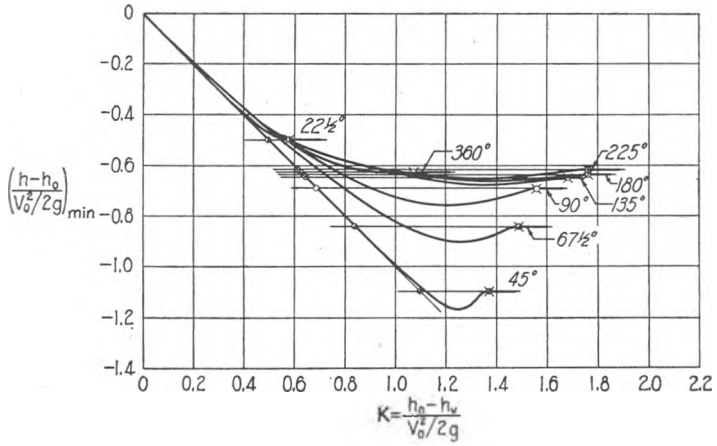

FIG. 22. VARIATION OF MINIMUM PRESSURE WITH CAVITATION INDEX FOR CONICAL HEAD FORMS.

nounced tendency for the pressure to drop for slight cavitation. The only exceptions in this series were the gently tapered 22½° form and the hollow cylinder. Since the latter also fails to follow the systematic trend whereby $\mathbf{K}_i$ increases with apex angle, the experimental results were carefully checked. Although no errors were found in the experiments, it was noted that the drop in pressure tended to decrease with increasing angle, leading perhaps to an imperceptible decrease for the 360° head and an indeterminate value for $\mathbf{K}_i$. A similar result will be noted for the concave ellipsoidal head.

These trends may also be seen in Fig. 23, in which both the minimum pressure ratio and the value of $\mathbf{K}_i$ are plotted against the apex angle, the uncertain region for the latter function being shown as a broken line. As the apex angle increases, the minimum pressure decreases until a more stable form of separation counteracts this tendency, eventually yielding a minimum pressure which is

essentially independent of the apex angle. Minimum-pressure conditions for the conical series are seen to occur at an apex angle of about 45°, tests on the 45° conical head form having shown, however, that flow conditions were sensitive to variation in the Reynolds number to the extent that the minimum pressure could not be exactly determined.

Essentially the same comments with respect to the pocket silhouettes apply to the conical as to the rounded series, and detailed profiles will again be found in the Appendix. Noteworthy is the

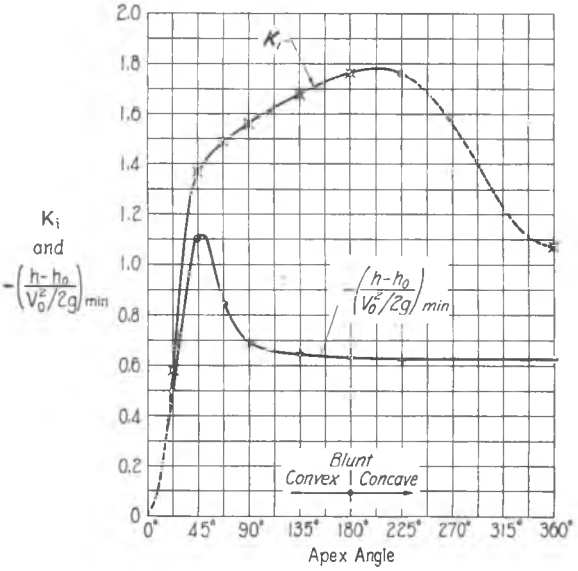

FIG. 23. CAVITATION INDEX AND MINIMUM PRESSURE VERSUS APEX ANGLE FOR INCIPIENT CAVITATION.

fact that boundary angularity now controls the point of separation rather than boundary-layer development along a continuous curve.

Ellipsoidal Series

For the third series of head forms, semi-ellipsoids of revolution were combined with the parallel afterbody, the various profiles within the series being characterized by the ratio of the longitudinal to the transverse axis of the generating ellipse. From Fig. 15 it may be seen that axis ratios of 4:1, 2:1, 1:1 (hemispherical), $\frac{1}{2}$:1, 0:1 (blunt), $-\frac{1}{2}$:1 (concave), and $-\infty$:1 (hollow cylindrical) were studied.

The mathematical simplicity of the ellipsoidal shape has long since made possible a solution for the pressure distribution around ellipsoids of revolution in irrotational flow. Although the afterparts of these bodies differ from those tested, the results of this analysis were found to agree closely with the experimental data for the longer forms. Based on the analyses presented by Durand [6] and Lamb [7], the following equations have been derived: For ovary ellipsoids (longitudinal axis greater than the maximum diameter) the velocity at any point on the surface is given by

$$v = V_0 \sin \alpha \left(\frac{e^2}{1 - A} \right)$$

where α is the angle between the direction of flow and a line normal to the profile, e is the eccentricity $\sqrt{a^2 - b^2}/a$ of the elliptical cross section and $A = \frac{1 - e^2}{2e} \ln \frac{1 + e}{1 - e}$. For planetary ellipsoids (longitudinal axis less than the maximum diameter) the corresponding relationship is

$$v = V_0 \sin \alpha \left(\frac{e^2}{B - 1 + e^2} \right)$$

where $B = \frac{\sqrt{1 - e^2}}{e} \sin^{-1} e$. For any ellipsoid (including the special case of the sphere and the limiting case of the circular disk) the expression for the pressure-distribution parameter reduces therefore to the form

$$\frac{h - h_0}{V_0^2/2g} = 1 - (k \sin \alpha)^2$$

The values of k are evidently constant for a given head form, since they are functions of the eccentricity (or axis ratio a/b) alone.

A second analytical solution for flow past the longer ellipsoidal forms was completed using the approximate method introduced by von Kármán [8]. If a number of sources and sinks are used in combination with a uniform velocity field, it is possible so to determine their intensities that one stream line of the resulting flow approaches a predetermined boundary profile. In this way analytical results were obtained for boundaries closely approximating the 4:1 and 2:1 semi-ellipsoidal forms with parallel afterbodies.

The pressure distributions from the two types of analysis are compared with the experimental results in Fig. 24, and indicate the agreement to be expected between theory and experiment for

the various axis ratios. The von Kármán method gives results for the longer forms which coincide almost exactly with experiment. The results from the first method of analysis also indicate good agreement for the longer forms, particularly near the nose. The departure near the point of tangency for such forms is primarily due to the basic difference in boundary form. The more general disagreement for the shorter forms, on the other hand, is the result of viscous effects which were ignored in the analysis and produce separation in the actual flow.

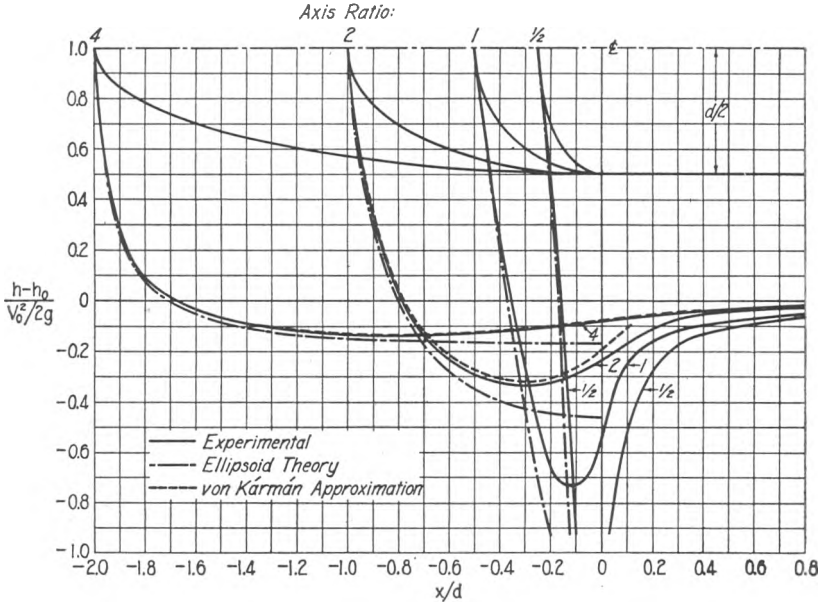

FIG. 24. COMPARISON OF ANALYTICAL AND EXPERIMENTAL PRESSURE DISTRIBUTIONS FOR ELLIPSOIDAL HEAD FORMS.

Fig. 25 represents the sequence of experimental pressure-distribution curves for the ellipsoidal heads at values of **K** above that for incipient cavitation, and at Reynolds numbers high enough to insure stable flow. As in the preparation of Figs. 16 and 21, experimental inconsistencies have been eliminated by adjusting intercept values on auxiliary plots. These plots, together with the analytical methods illustrated by Fig. 24, were readily adaptable to the determination of pressure curves for the intermediate axis ratios included in Fig. 25. The interpolated values are reasonably accurate throughout, except for axis ratios of $\frac{3}{4}$ and $\frac{1}{4}$. As in the case

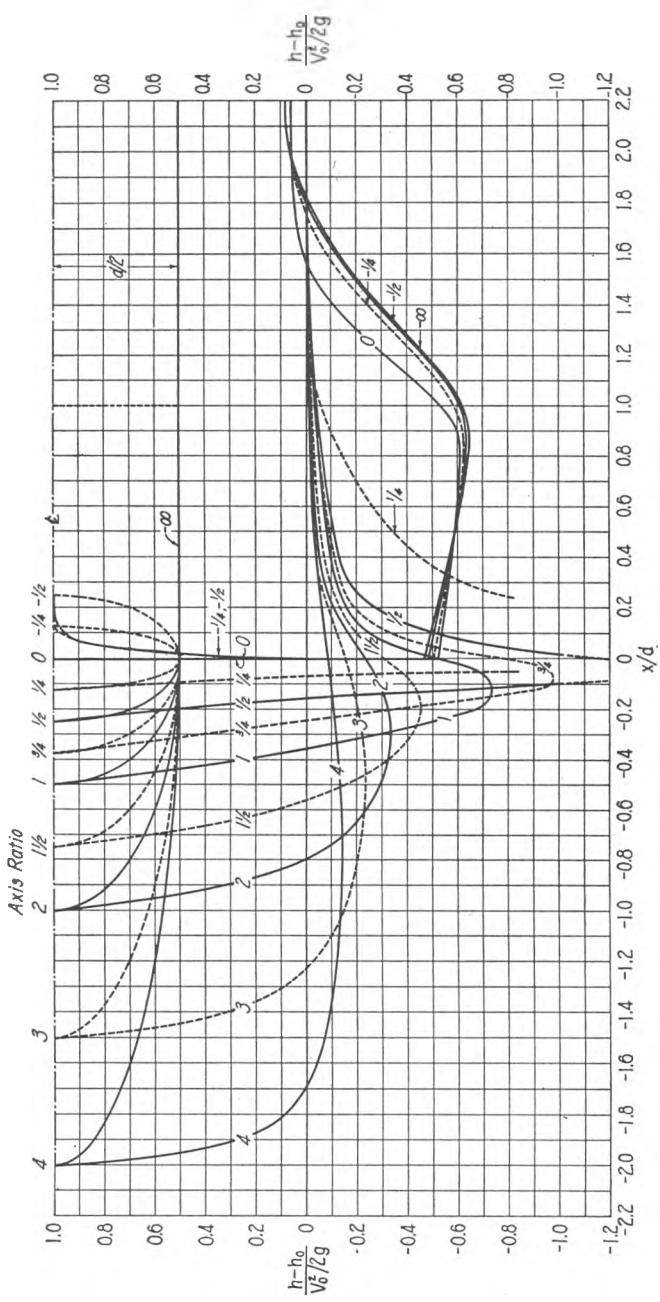

FIG. 25. LONGITUDINAL DISTRIBUTION OF PRESSURE FOR THE ELLIPSOIDAL SERIES AS A FUNCTION OF AXIS RATIO.

of the $\frac{1}{8}$-caliber rounded head, the $\frac{1}{2}$:1 ellipsoid showed a pronounced variation with the Reynolds number throughout the range of the tunnel, the uncertainty of the results for this head making interpolation to the adjacent axis ratios uncertain as well.

Figs. 26 and 27 show the interrelationship between the minimum

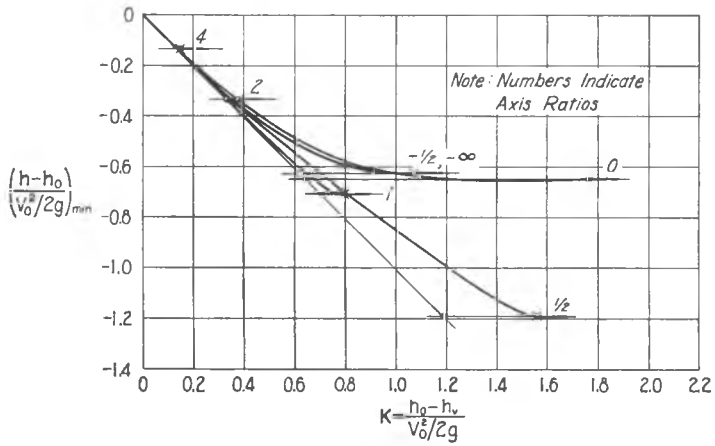

FIG. 26. VARIATION OF MINIMUM PRESSURE WITH CAVITATION INDEX FOR ELLIPSOIDAL HEAD FORMS.

pressure ratio, the axis ratio of the ellipsoidal head forms, and **K**. These two figures, together with Fig. 25, bear out trends observed in the other series; the longer, well-faired shapes show, in addition to the expected slight decrease in local pressure, a tendency for the minimum pressure ratio to equal the value of **K**, both in the cavitation range and at incipient cavitation. At the other extreme the blunt and concave forms illustrate conflicting trends for the larger **K** values, only the blunt form yielding the dip in the pressure curve and the resulting increase in $\mathbf{K}_i$ which was general for the conical series.

The theoretical limit in Fig. 27(b), which was obtained from the analysis of flow past ellipsoids of revolution, serves to define the extension of the two curves. This upper limit, together with the trend of the neighboring points, also decreases the possible error in the uncertain results for the $\frac{1}{2}$:1 form. The theoretical line, which is actually a combination of two curves for the two types of ellipsoid, closely approaches a straight line within the region of interest.

Supplementary Series

First in a series of supplementary shapes also investigated was a single head having the form of the mathematical half body. This form was considered significant because of its definition as a natural fluid boundary, and the likelihood that such a boundary would have a comparatively slight tendency toward cavitation. In addition, these tests offered further opportunity to check experimentally the accuracy of the flow pattern predicted by a theoretical analysis.

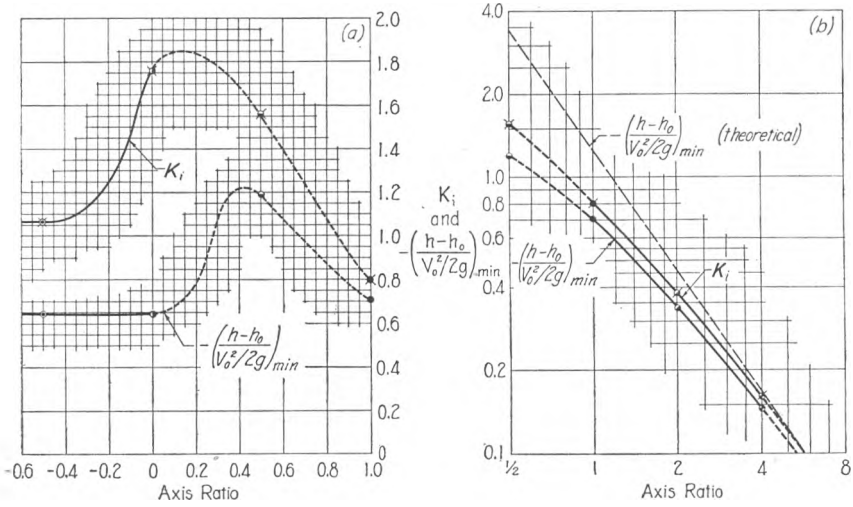

FIG. 27. CAVITATION INDEX AND MINIMUM PRESSURE VERSUS AXIS RATIO FOR INCIPIENT CAVITATION.

The surface of the mathematical half body is defined by the streamlines passing through the stagnation point in fluid moving with an initially uniform velocity past a three-dimensional point source [9]. The equation of this boundary in polar coordinates may be written in the form

$$4\,r\,\sin\frac{\theta}{2} = d_0$$

where d_0 is the maximum diameter which the body approaches asymptotically as the angle θ becomes small. As it was obviously impossible to extend this boundary form to the mathematical limit, the value of d_0 was made one percent greater than the one-inch radius of the cylindrical shaft, and the half-body profile was extended only until it intersected the profile of the cylindrical shaft.

As a result there was an abrupt although very slight change in profile at a point immediately downstream from piezometer number 12 about 2 diameters from the nose.

The theoretical pressure distribution around a half body, as determined from the velocity potential of the combined flow, can be expressed in terms of either r or θ:

$$\frac{p - p_0}{\rho V_0^2/2} = \left(\frac{d_0}{4r}\right)^2 \left[3\left(\frac{d_0}{4r}\right)^2 - 2\right]$$

$$= \sin^2\frac{\theta}{2}\left(3\sin^2\frac{\theta}{2} - 2\right)$$

The corresponding curve is compared with the experimental results in Fig. 28. The agreement between theory and measurement is seen to be good throughout the entire range. The magnitude of the minimum pressure, its point of occurrence, and the distribution of pressure upstream therefrom agree so closely that only a

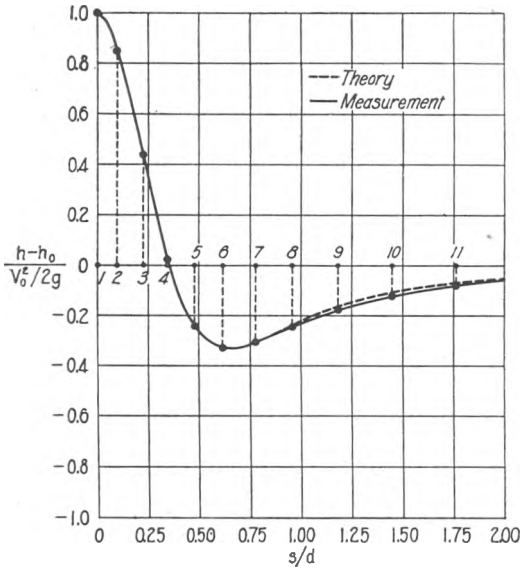

FIG. 28. COMPARISON OF EXPERIMENTAL AND THEORETICAL PRESSURE DISTRIBUTIONS FOR THE HALF-BODY TORPEDO HEAD.

single curve could be drawn. In the region of decelerated flow immediately downstream, a noticeable but still slight discrepancy was found, indicating a limited zone of separation or boundary eddies. It is difficult to compare the half body with other profiles, since either a longer or a shorter half-body head, brought to the 1-inch

diameter in the manner already described, would be expected to give essentially the same minimum pressure. Although the length as constructed is somewhat greater than the 2:1 ellipsoidal form, the minimum pressure is approximately the same.

Two other types of head were subsequently tested in order to determine the effect on the cavitation characteristics of a systematic variation in profile form with a constant ratio of profile length to diameter. In other words, for a particular length-diameter ratio a head form was sought for which the tendency toward cavitation would be reduced to a practicable minimum. Although considerable emphasis has already been given to the fact that the minimum pressure ratio is not even approximately equal to $\mathbf{K}_i$, it may be seen from Figs. 18 and 27 that the two values are proportional for the longer forms, differing by approximately 10%. It follows that a reduction in the minimum pressure ratio would yield a comparable reduction in $\mathbf{K}_i$.

As the hemispherical head form was used as the basis of comparison for the first type, the variations therefrom have been described as modified hemispherical heads. Since this basic form has a constant radius of curvature, it was thought that a reduction in the pressure drop near the circle of tangency could be secured through an increase in the radius of profile curvature in this zone and a corresponding decrease near the tip.

A study of the general profile equation

$$\left(\frac{2x'}{d}-1\right)^m+\left(\frac{2r}{d}\right)^n=1$$

(in which x' and r are the profile coordinates in cylindrical notation, x' differing from x in that it is measured from the nose rather than from the point of tangency) indicated that through proper choice of exponents the relative curvature at nose and point of tangency could be controlled to a considerable degree. For instance, if m is held constant at the value 2 and n is successively increased from 2 (for the hemisphere) to 3, 4, and 5, the profile sequence of Curves I, II, III, and IV of Fig. 29 will result.

Since the radius of curvature at the point of tangency becomes successively greater, it appears reasonable to assume that the zone of minimum pressure intensity should be shifted farther and farther from the point of tangency, and hence that the pressure reduction should become correspondingly less extreme. On the other

hand, holding the exponent n constant at the value 2 and increasing m (as for Curve V) should produce the opposite effect.

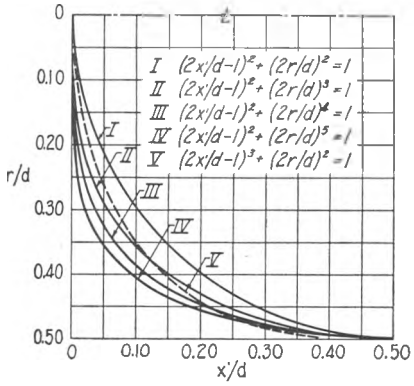

FIG. 29. PROFILES OF MODIFIED HEMISPHERICAL HEAD FORMS.

Measurements made in the water tunnel for each of the profiles in question provided data for the composite plot of Fig. 30 for non-cavitating conditions. Curve V, as was to be expected, evidences a minimum value which is markedly lower than that for the hemisphere (Curve I). Curves II, III, and IV likewise indicate the

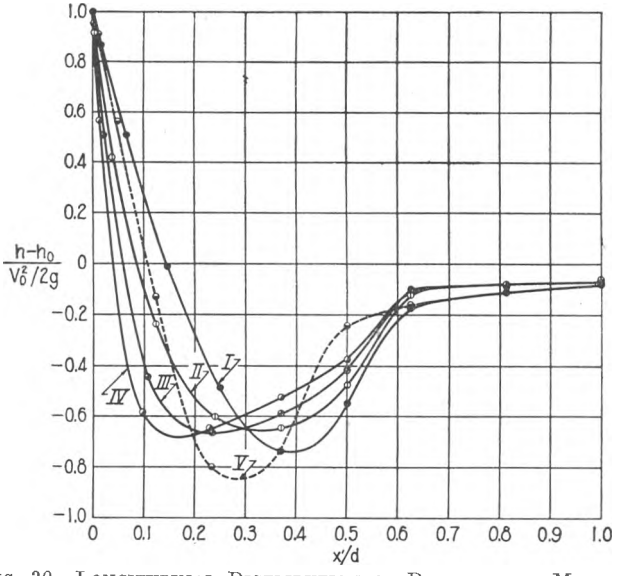

FIG. 30. LONGITUDINAL DISTRIBUTION OF PRESSURE ON MODIFIED HEMISPHERICAL HEADS.

expected progressive shift in the point of minimum pressure toward the zone of decreased radius of curvature. The corresponding reduction in the pressure drop, on the other hand, is disappointingly slight. In fact, the indicated magnitude of $\mathbf{K}_i$ is reduced only 10% below that for the hemisphere, and this maximum reduction is obtained for Curve II rather than III or IV.

In the belief that a profile curve not restricted by the exponential function of the modified hemispherical forms might still result in an improvement in the pressure distribution and a corresponding reduction in $\mathbf{K}_i$, another type of head form was tested. This series consisted of blunt noses with ellipsoidal transitions as shown in Fig. 31, and is therefore referred to as the modified ellipsoidal. Part of

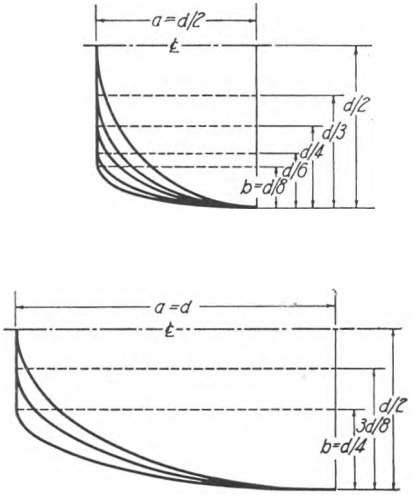

FIG. 31. PROFILES OF MODIFIED ELLIPSOIDAL HEAD FORMS.

the series, having a ratio of profile length to profile diameter of $\frac{1}{2}$:1, is comparable to both the hemispherical and modified hemispherical forms; the other, with a ratio of unity, approaches the 2:1 ellipsoidal form as a limit. The distributions of pressure around the shorter forms for non-cavitating conditions are shown in Fig. 32 and around the longer forms in Fig. 33. In each case a decrease in the transverse dimension b of the curved portion is accompanied by a progressive shift of the point of minimum pressure toward the nose, a logical consequence of the increase in curvature near the nose and the corresponding decrease in the region near the

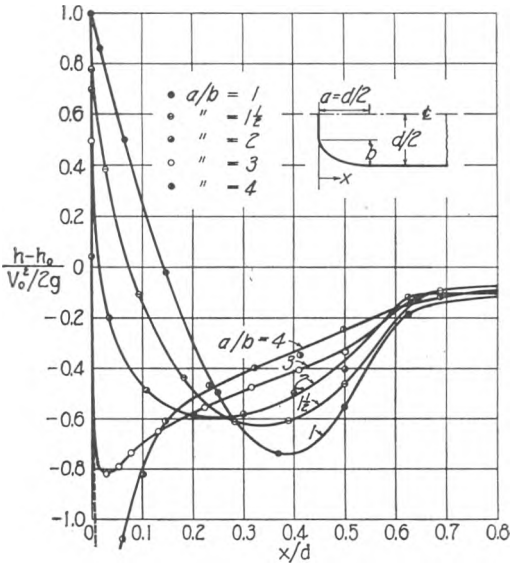

FIG. 32. LONGITUDINAL DISTRIBUTION OF PRESSURE FOR MODIFIED ELLIPSOIDAL HEADS ($a = d/2$).

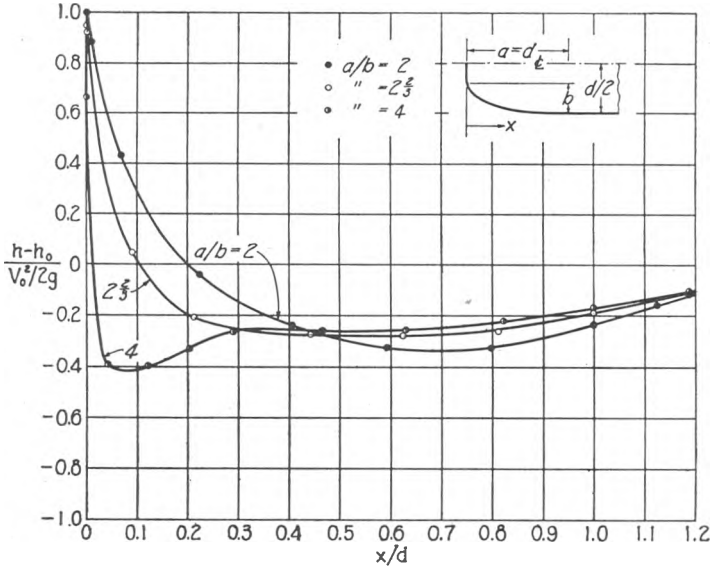

FIG. 33. LONGITUDINAL DISTRIBUTION OF PRESSURE FOR MODIFIED ELLIPSOIDAL HEADS ($a = d$).

parallel section. The maximum drop first decreased with increase in the blunt area, and then increased as the curvature near the juncture with the blunt nose became extreme, very low pressures occurring at small values of b.

In order to generalize the results, a plot of the minimum-pressure ratio versus $2b/d$ was prepared for the two series and is presented in Fig. 34 together with single points from the $\frac{1}{4}$-caliber rounded and the 4:1 ellipsoidal heads. From this rather limited information and the logical conclusion that for $2b/d = 1$ the minimum pressure would approach zero asymptotically with increasing a/d, the broken line was drawn to assist in interpolation to other values of a/d than

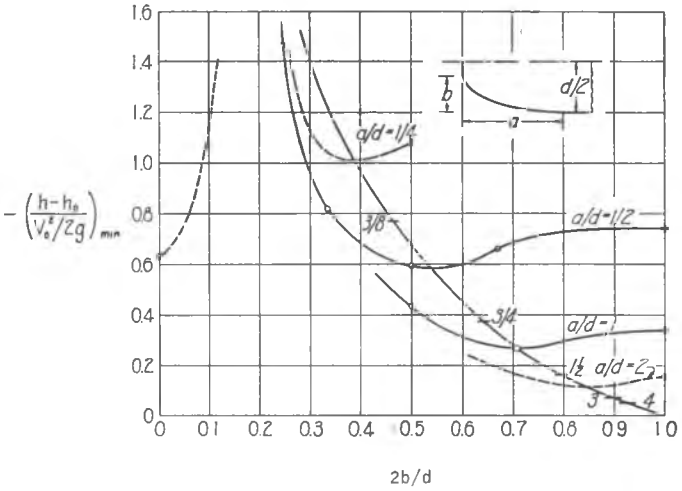

FIG. 34. DISTRIBUTION OF MINIMUM PRESSURE WITH MODIFIED ELLIPSOIDAL HEAD FORM.

those tested. Although relatively few points were used in defining this curve, it is thought to be quite accurate for values of a/d equal to or greater than $\frac{1}{2}$, the interpolated values having been obtained from an auxiliary plot of the minimum pressure ratio against a/d. On the other hand, for values of a/d less than $\frac{1}{2}$ the location of the curve becomes increasingly uncertain, particularly since a pronounced separation will undoubtedly occur for the very short forms.

It is concluded that the modified ellipsoids represent a considerable improvement over other forms of comparable length-diameter ratios with regard to the tendency toward cavitation. In each of the two cases, the maximum pressure drop was reduced by nearly 20%, thus permitting an increase of nearly 10% in the maximum

velocity which may be attained without cavitation. It is also noteworthy that the forms are simply defined, and possess a larger volume than those which are completely faired. Since the blunt nose has been found to have a stabilizing influence under conditions of water entry, it is of particular interest to note the considerable degree to which the ratio a/d may be varied without affecting greatly the magnitude of $\mathbf{K}_i$. The modified-ellipsoidal profile, in other words, is readily subject to alteration in specific form to satisfy criteria other than low susceptibility to cavitation.

V. SUMMARY OF RESULTS

Essential to the final evaluation of any series of experiments is knowledge of the extent to which the desired test conditions have actually been achieved. For the experiments described herein, the production of uniform pressure and velocity in the test section, the attainment of stable Reynolds-number regimes, and the elimination of air-content effects upon the cavitation phenomenon were of primary importance. The results of preliminary studies of these factors may be summarized as follows:

1. Despite noticeable non-uniformities of velocity in the approaching flow, both the velocity and the pressure in the open-throat test section varied less than $\frac{1}{2}\%$ from their mean values throughout the region of experimental interest. Introduction of a throat enclosure practically eliminated this variation. However, whereas the enclosure resulted in appreciable errors in the pressure distribution around test forms occupying only 2% of the flow section, in the open throat such effects could not be noted even with forms obstructing as much as 10% of the cross-sectional area.
2. No influence of dissolved air upon cavitation was discernible as long as the pressure in the test section was somewhat above that of the preceding de-aeration run, but operation of the tunnel at lower pressures (the cavitation number remaining the same) yielded a change in the pressure distribution around test forms not unlike that resulting from a change in the cavitation number. To eliminate error it was therefore concluded that the operating pressure should be at least 0.5 foot of water above the de-aeration pressure.
3. As in previous investigations on boundary flow, a critical Reynolds number was found to define the upper limit of

viscous effects upon the flow pattern for any given form of body. This critical value varied considerably with body geometry, and in some cases lay beyond the range of the tunnel ($\mathbf{R} = 5 \times 10^5$). Noteworthy is the fact that the highest critical Reynolds numbers corresponded to bodies of intermediate length — the longer profiles eliminating the tendency for flow to separate from the boundary and the blunter profiles producing early formation of a stable separation zone. In order to simulate flow patterns to be expected at high Reynolds numbers of prototype conditions, it was therefore evident that all tests should be conducted at values of $\mathbf{R}$ well above the upper critical for the body form in question.

Subsequent determination of the pressure distribution around 31 different heads of rounded, conical, ellipsoidal, and modified forms at various degrees of cavitation led to systematic families of distribution curves, the most significant characteristics of which may be summarized as follows:

1. The greatest local reduction in pressure occurred on intermediate forms in each of the three major series: the $\frac{1}{8}$-caliber rounded, the 45° conical, and the $\frac{1}{2}$:1 ellipsoidal. In the case of longer forms, owing to the reduced tendency toward separation, the pressure drop was more gradual and much less extreme. In the case of blunter forms, the presence of a stable zone of separation not only reduced the pressure drop but also resulted in essentially constant pressure throughout the separation zone. The form of this zone was clearly indicated by photographs taken under conditions of mild cavitation.
2. Close agreement was obtained between the measurements for the well faired forms and computations based upon the assumption of irrotational flow — the longer semi-ellipsoids and the half-body form providing a ready basis for comparison. Hence it may be concluded that analytical methods may be used to evaluate the pressure distribution under conditions of negligible separation. Further analyses based upon simplified boundary conditions proved useful guides in systematizing and extending experimental results.
3. In every instance the first effects of cavitation upon the boundary pressure distribution occurred before the latter had

reached the vapor pressure, owing to prior formation of cavities within the fine-scale eddies in the boundary layer or along the surface of separation. As a result, prediction of $\mathbf{K}_i$ from the minimum pressure under cavitation-free conditions can be at best an approximation, and will in some cases be greatly in error. For the faired boundaries the difference was found to be a matter of some 10%, but for the blunter forms the minimum pressure head at the boundary was as much as one velocity head above the vapor pressure head when cavitation along the surface of separation first affected the pressure distribution, the actual magnitude of $\mathbf{K}_i$ then being nearly 200% greater than that predicted. Surprisingly, the initial change in the latter cases was usually a reduction in boundary pressure.

4. Further decrease in the value of **K** led in every case to the eventual establishment of a cavitation zone in which the boundary pressure was essentially constant and equal to the vapor pressure, the length and diameter of the pocket increasing with reduction in the value of **K**. Immediately downstream from this zone the pressure rose rapidly to a higher value than for flow without cavitation, a logical result of the existence of flow toward the boundary in this region. Still farther downstream the pressure returned to the undisturbed value. A systematic relationship between the mean pressure distribution and the mean pocket silhouette was found to exist.
5. In an attempt to determine the profile form least likely to produce cavitation, studies were made of several modified forms with a given length-diameter ratio. Although only a few of the many possible forms were investigated, a simple combination of a partially blunt nose with an elliptical transition was found to give results considerably better than the others tested. For a length-diameter ratio of $\frac{1}{2}$:1, the blunt portion of the nose being one-half the diameter of the shaft, a minimum pressure ratio nearly 20% above that of the hemisphere was obtained. Corroborative tests for longer head forms produced comparable results.

ACKNOWLEDGEMENTS

The major part of the present summary, as well as the experimental tests reproduced herein, was completed by the Institute under Contract NObs-24084 with the U. S. Navy Bureau of Ships. The initial program was outlined by Captain H. E. Saunders, then Technical Director of the David Taylor Model Basin, who continued active sponsorship of the investigation during his subsequent year as Model Basin Director. Completion of the manuscript, as well as its final publication, was sponsored by the Office of Naval Research under Contracts N7onr-495 and N8onr-500. All experiments and computations and much of the organization of results were carried out under the supervision of the authors by Messrs. En-Yun Hsu and Charles A. Lamb of the Institute staff. The very precise instrumentation and machining of the head forms was the handiwork of Mr. J. G. Sentinella of the University physics shop.

LIST OF REFERENCES

[1]. McNown, John S., "Pressure Distribution and Cavitation on Submerged Boundaries," Proceedings of the Third Hydraulics Conference, University of Iowa Studies in Engineering, Bulletin 31, 1947.

[2]. Knapp, Robert T., "Nose Cavitation — Ogives and Spherogives," OSRD Report 6.1-sr207-1906, California Institute of Technology, 1945.

[3]. Knapp, Robert T., and Hollander, A., "Laboratory Investigations of the Mechanism of Cavitation," Hydraulics Division ASME, December 1947.

[4]. Lamb, Horace, "Hydrodynamics," Sixth Edition, Dover Publication, New York, 1945, pp. 104-5.

[5]. Gauss, C. F., "Werke," Göttingen, Germany, 1870, Vol. III, p. 161.

[6]. Durand, W. F., "Aerodynamic Theory," Vol. I, pp. 277-292.

[7]. Lamb, Horace, "Hydrodynamics," pp. 139-144.

[8]. Kármán, Th. von, "Berechnung der Druckverteilung an Luftschiffkörpern" (Calculation of Pressure Distribution on Airship Hulls), Abhandlungen aus dem Aerodynamischen Institut an der Technischen Hochschule Aachen, 1927, No. 6. Translation in NACA Technical Memorandum 574, July 1930.

[9]. Rouse, Hunter, "Fluid Mechanics for Hydraulic Engineers," Engineering Societies Monographs, McGraw-Hill, 1938, pp. 89-90.

APPENDIX

LIST OF SYMBOLS

a, b	linear dimensions; major and minor axes of ellipse
d	diameter of parallel afterbody
D	diameter of jet
g	gravitation acceleration
h	piezometric head
h_a	partial-pressure head of air liberated from water
h_0	piezometric head in the undisturbed flow
h_v	vapor-pressure head of water
$\mathbf{K}$	cavitation index $\dfrac{h_0 - h_v}{V_0^2/2g}$
$\mathbf{K}_i$	incipient-cavitation index
p	pressure intensity
r	radius
$\mathbf{R}$	Reynolds number $V_0 d/\nu$
s	developed distance along boundary
v	velocity at any point
V_0	velocity of undisturbed flow
x	longitudinal distance from point of tangency
x'	longitudinal distance from nose
β	apex angle of conical head form
γ	specific weight
ν	kinematic viscosity
ϱ	mass density
φ	β/π

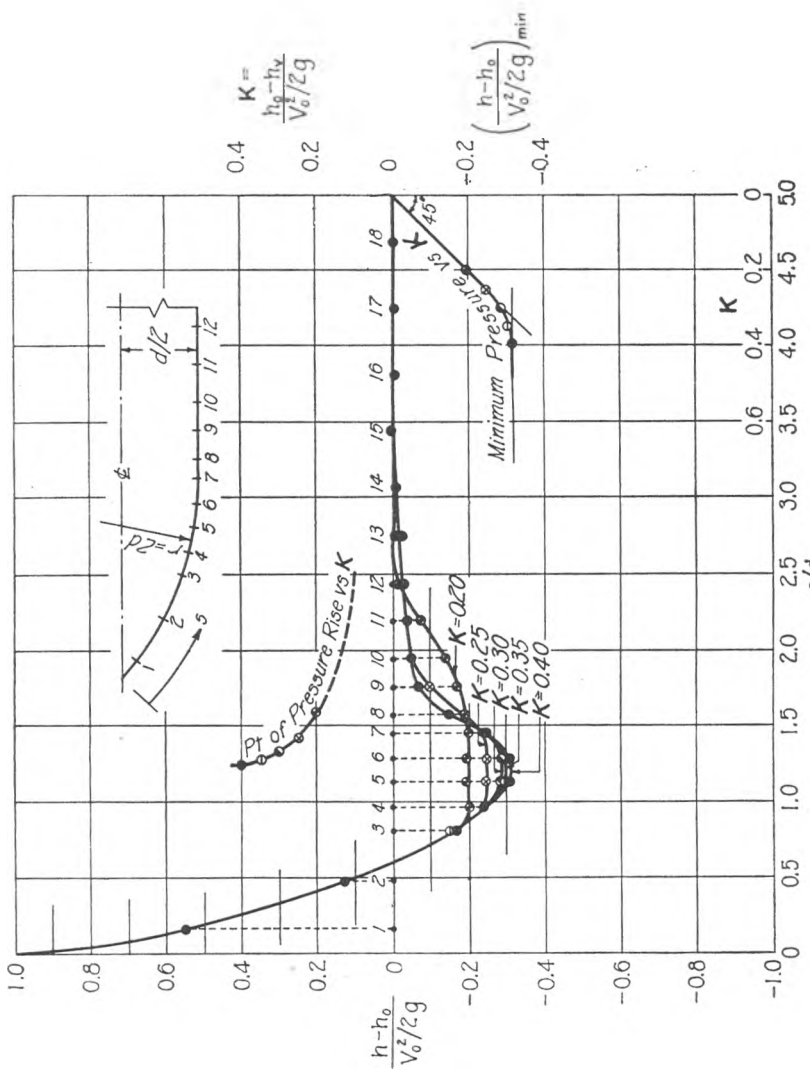

FIG. 35. EFFECT OF CAVITATION ON THE PRESSURE DISTRIBUTION AROUND A CYLINDRICAL BODY WITH A 2-CALIBER OGIVAL HEAD.

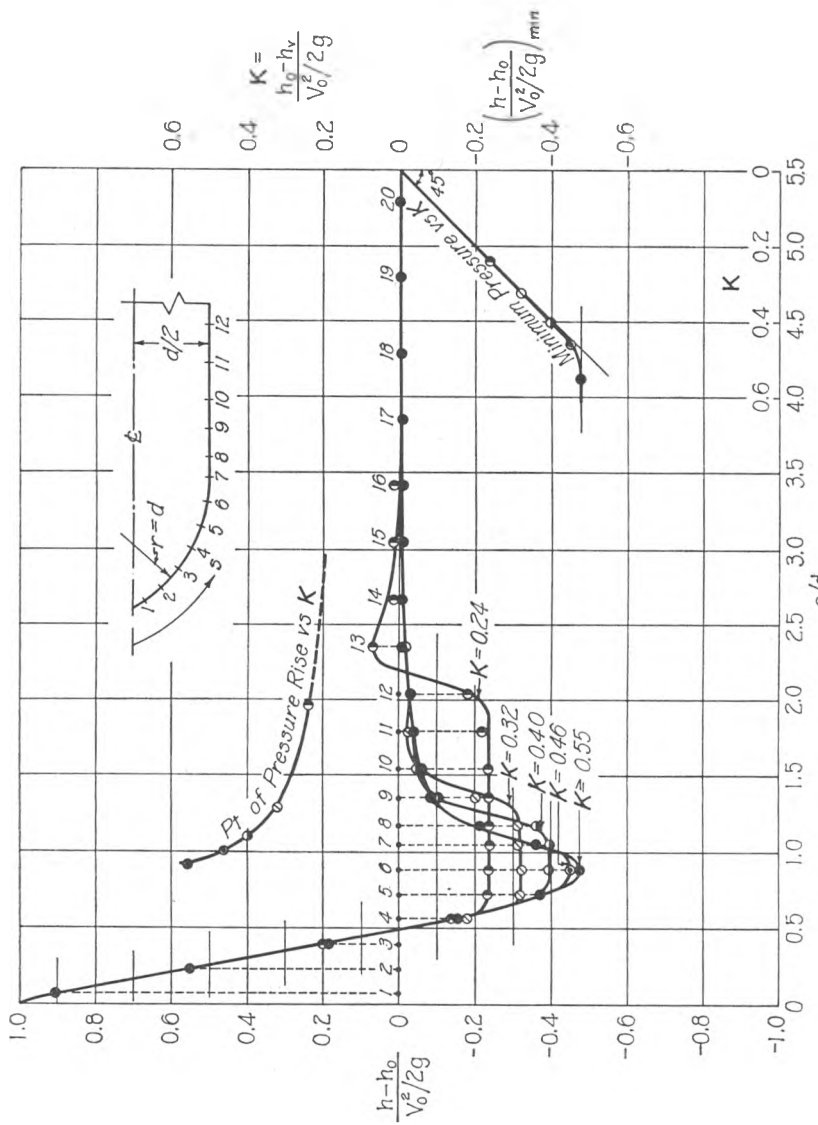

FIG. 36. EFFECT OF CAVITATION ON THE PRESSURE DISTRIBUTION AROUND A CYLINDRICAL BODY WITH A 1-CALIBER OGIVAL HEAD.

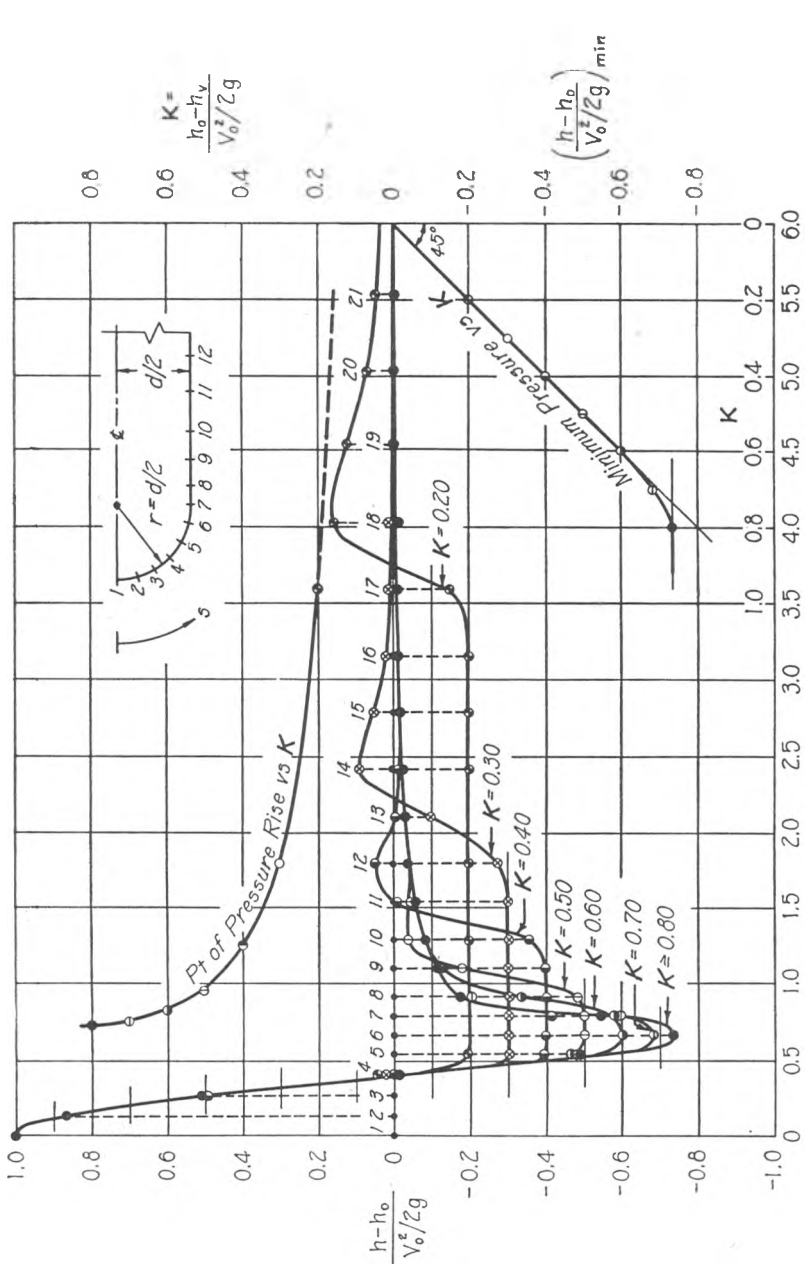

FIG. 37. EFFECT OF CAVITATION ON THE PRESSURE DISTRIBUTION AROUND A CYLINDRICAL BODY WITH A HEMISPHERICAL HEAD.

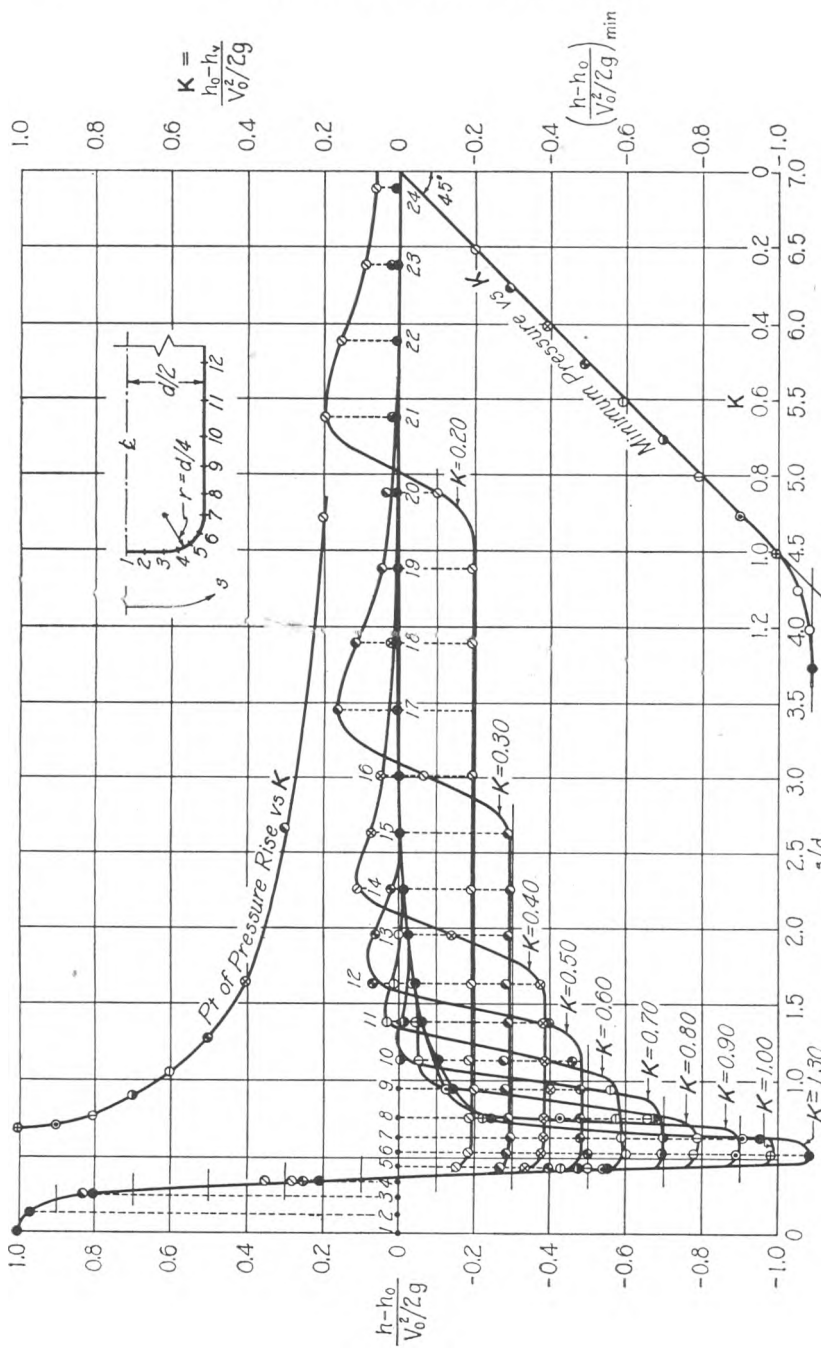

FIG. 38. EFFECT OF CAVITATION ON THE PRESSURE DISTRIBUTION AROUND A CYLINDRICAL BODY WITH A ¼-CALIBER ROUNDED HEAD.

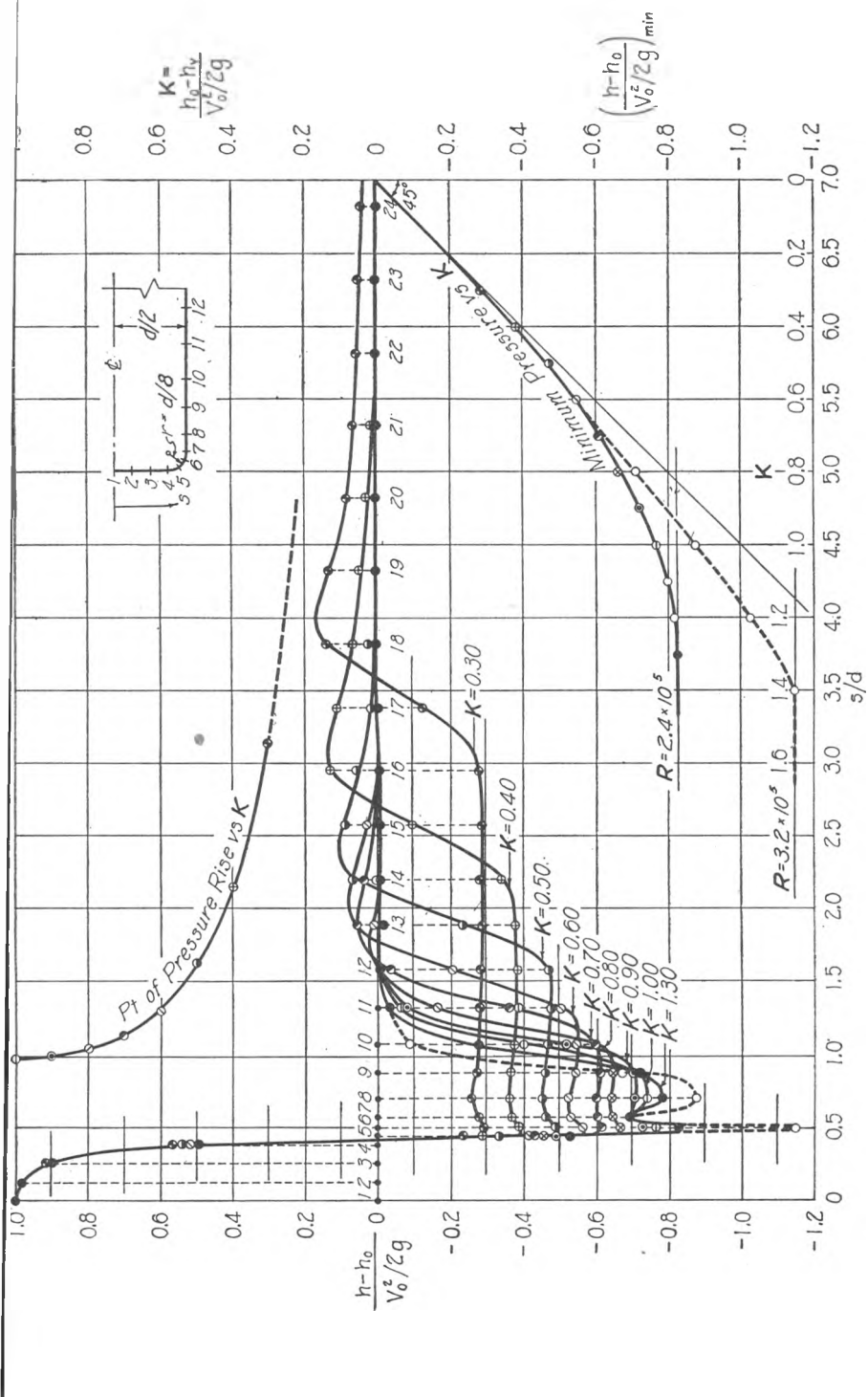

FIG. 39. EFFECT OF CAVITATION ON THE PRESSURE DISTRIBUTION AROUND A CYLINDRICAL BODY WITH A ¼-CALIBER ROUNDED HEAD.

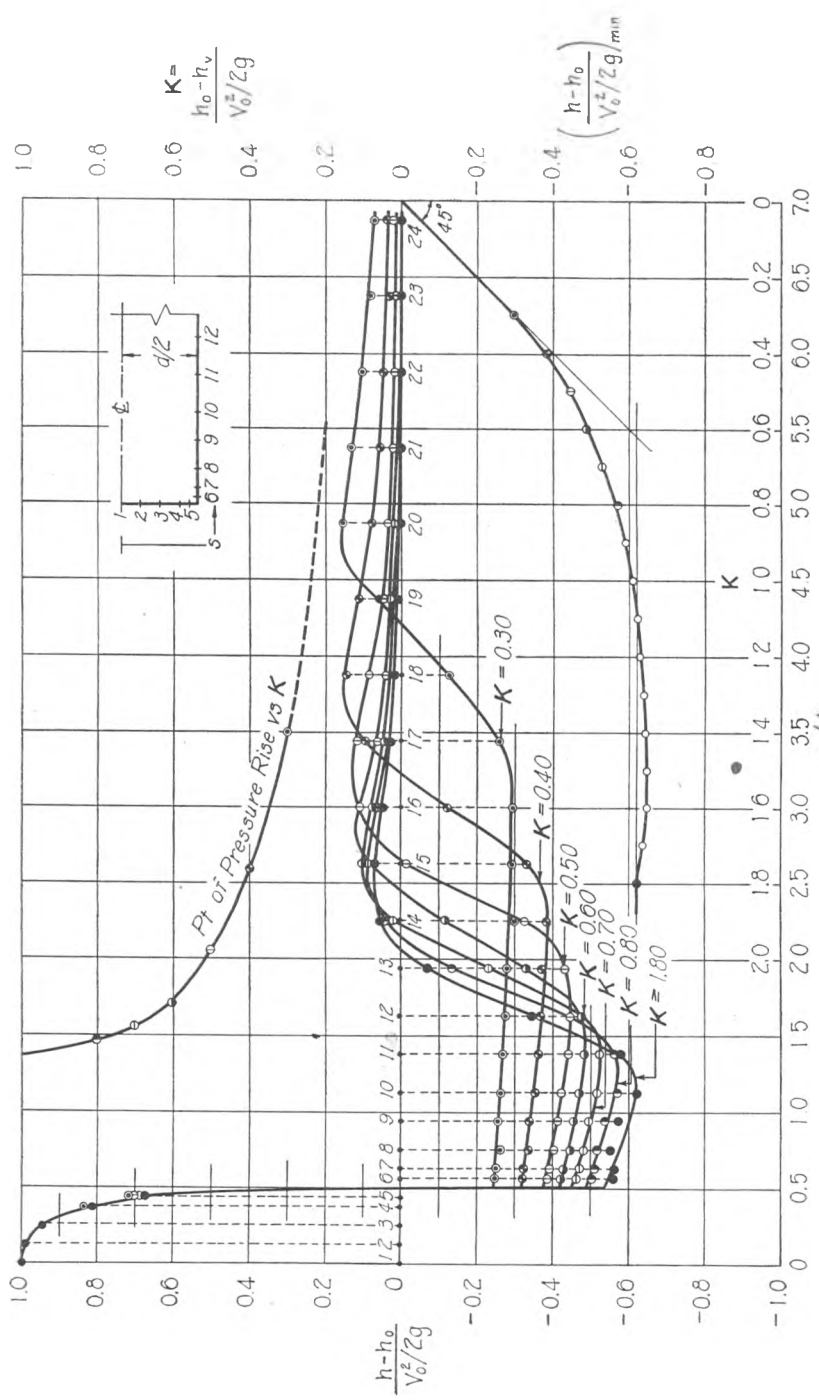

FIG. 40. EFFECT OF CAVITATION ON THE PRESSURE DISTRIBUTION AROUND A CYLINDRICAL BODY WITH A BLUNT HEAD.

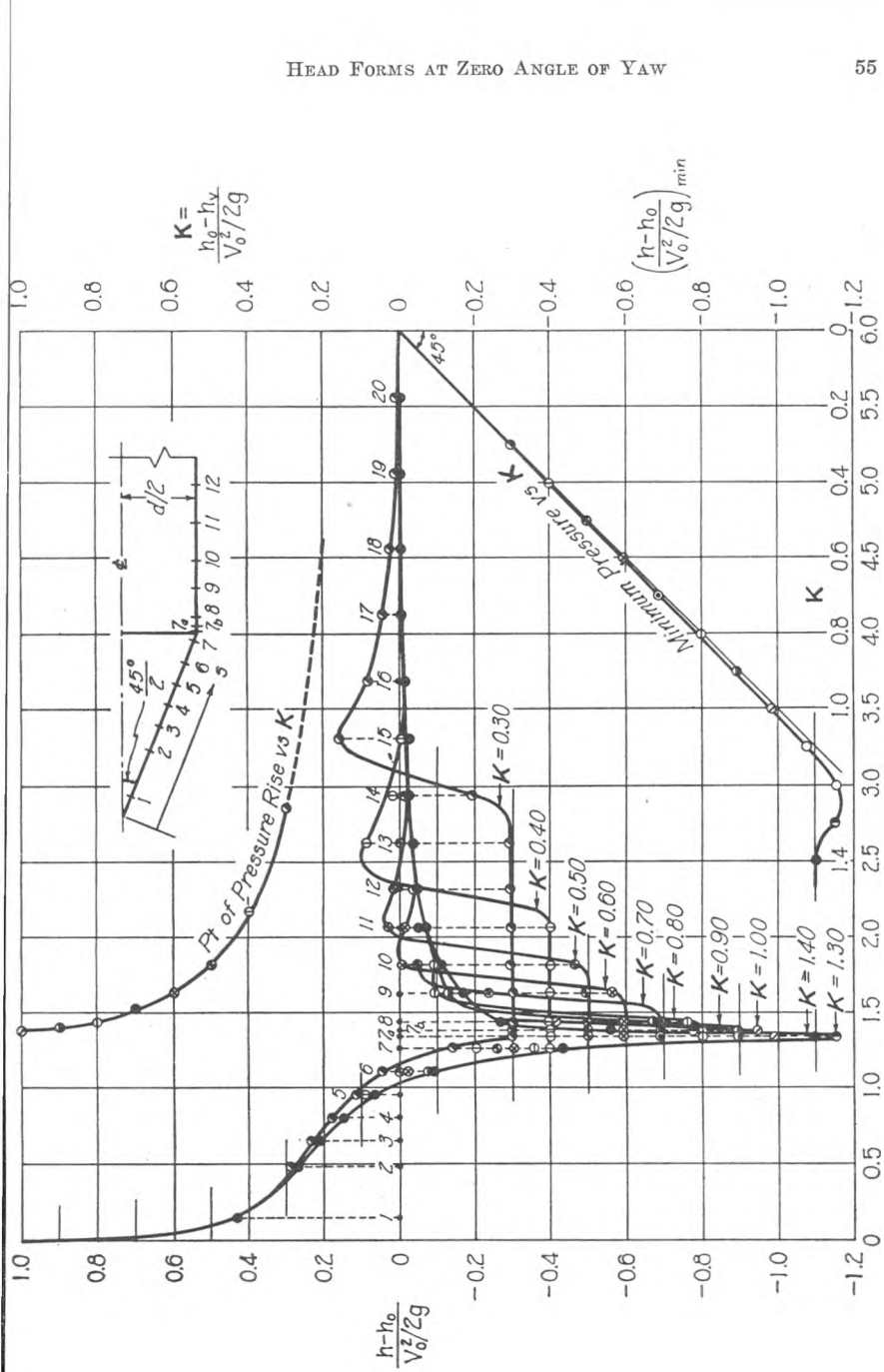

FIG. 41. EFFECT OF CAVITATION ON THE PRESSURE DISTRIBUTION AROUND A CYLINDRICAL BODY WITH A 45° CONICAL HEAD.

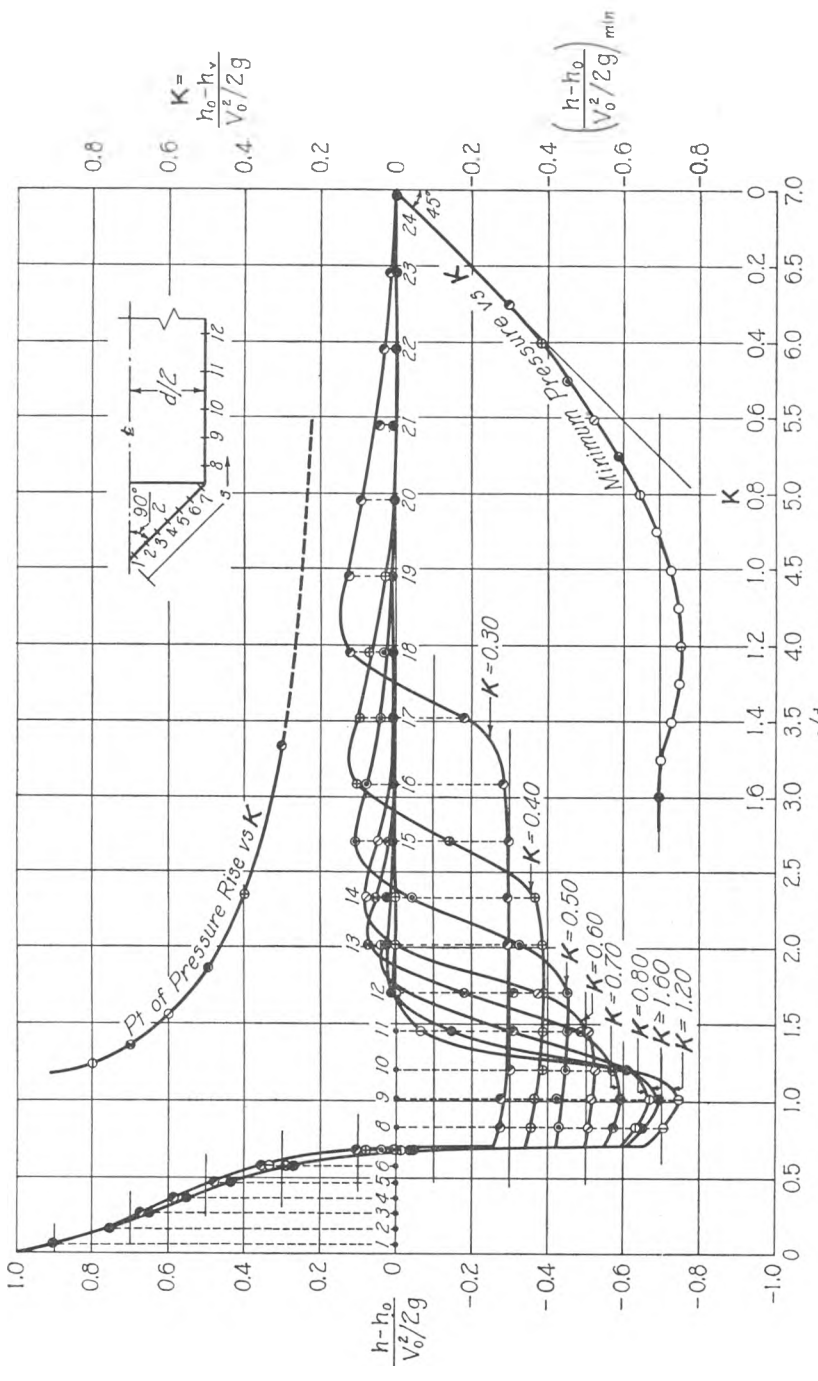

FIG. 42. EFFECT OF CAVITATION ON THE PRESSURE DISTRIBUTION AROUND A CYLINDRICAL BODY WITH A 90° CONICAL HEAD.

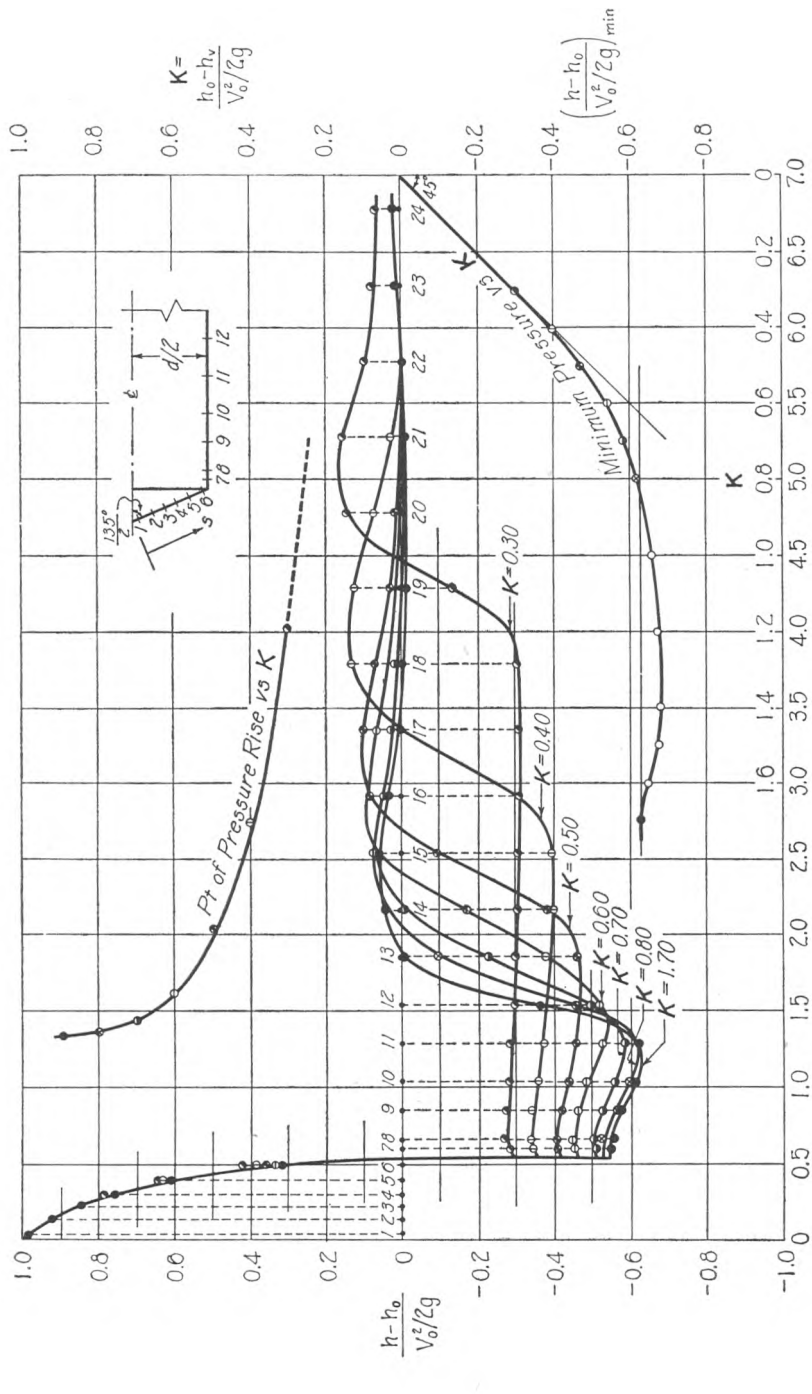

FIG. 43. EFFECT OF CAVITATION ON THE PRESSURE DISTRIBUTION AROUND A CYLINDRICAL BODY WITH A 135° CONICAL HEAD.

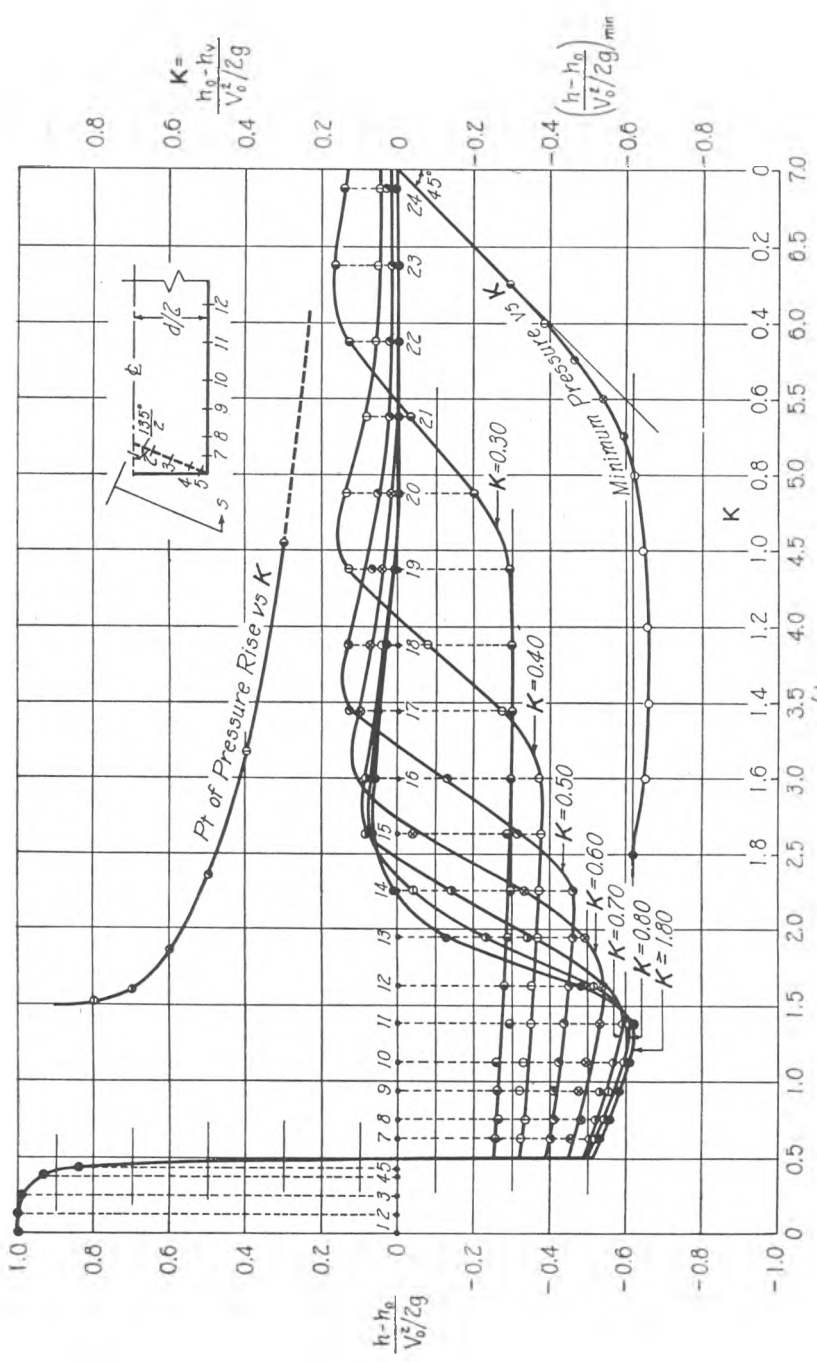

FIG. 44. EFFECT OF CAVITATION ON THE PRESSURE DISTRIBUTION AROUND A CYLINDRICAL BODY WITH A 135° CONCAVE CONICAL HEAD.

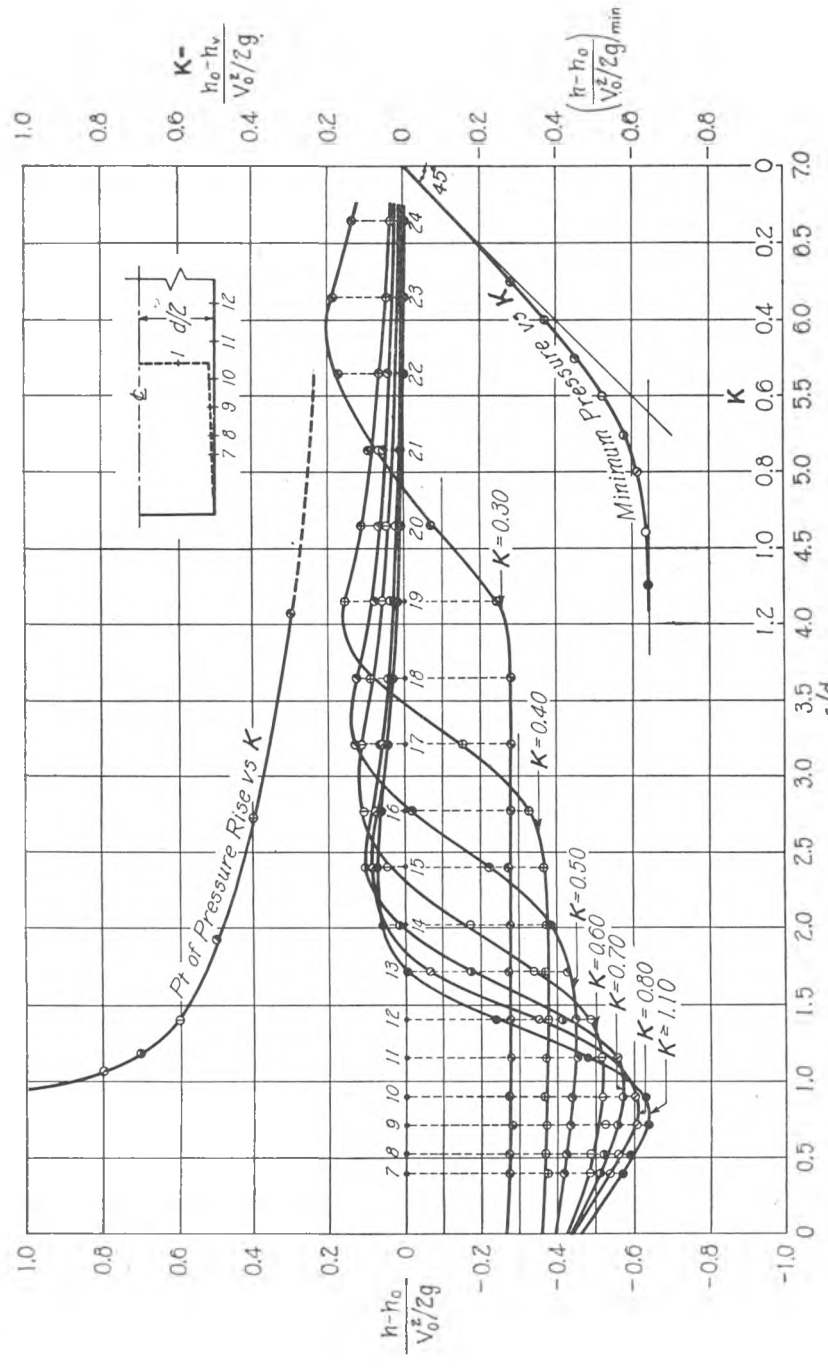

FIG. 45. EFFECT OF CAVITATION ON THE PRESSURE DISTRIBUTION AROUND A CYLINDRICAL BODY WITH A HOLLOW CYLINDRICAL HEAD.

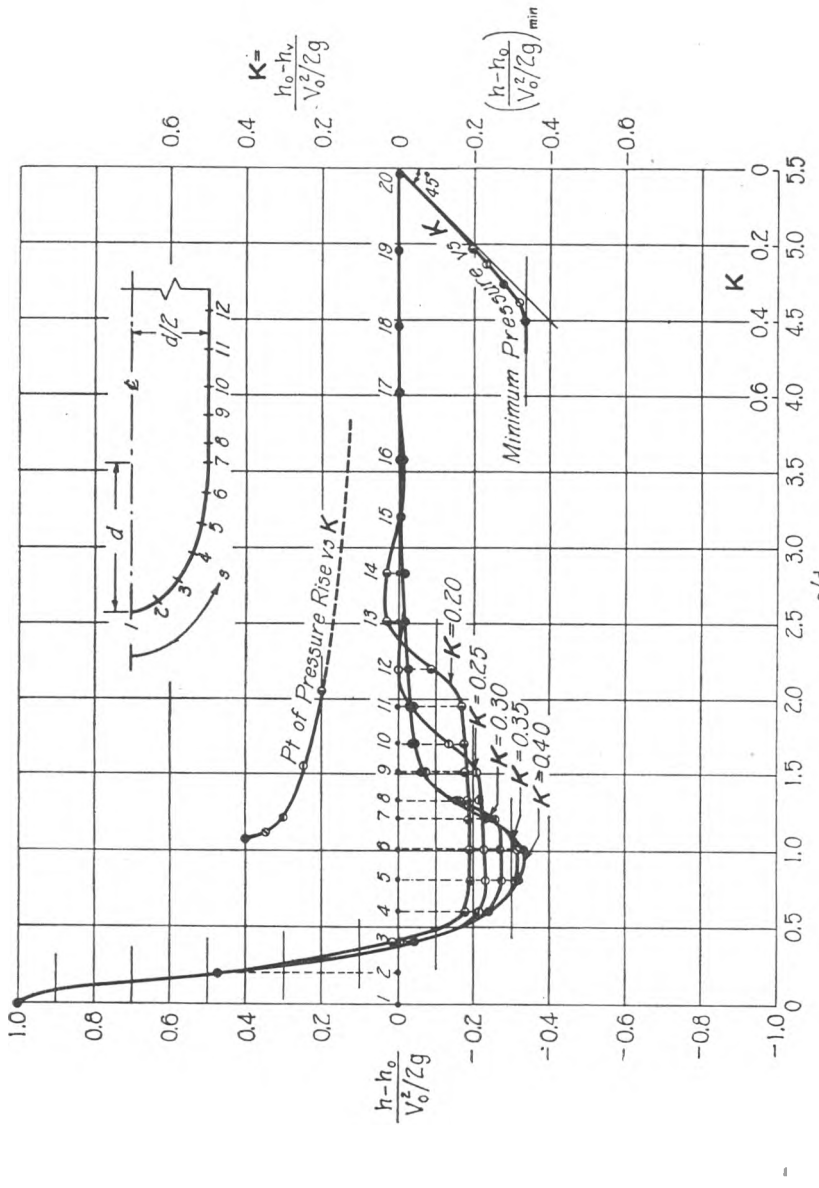

FIG. 46. EFFECT OF CAVITATION ON THE PRESSURE DISTRIBUTION AROUND A CYLINDRICAL BODY WITH A 2:1 ELLIPSOIDAL HEAD.

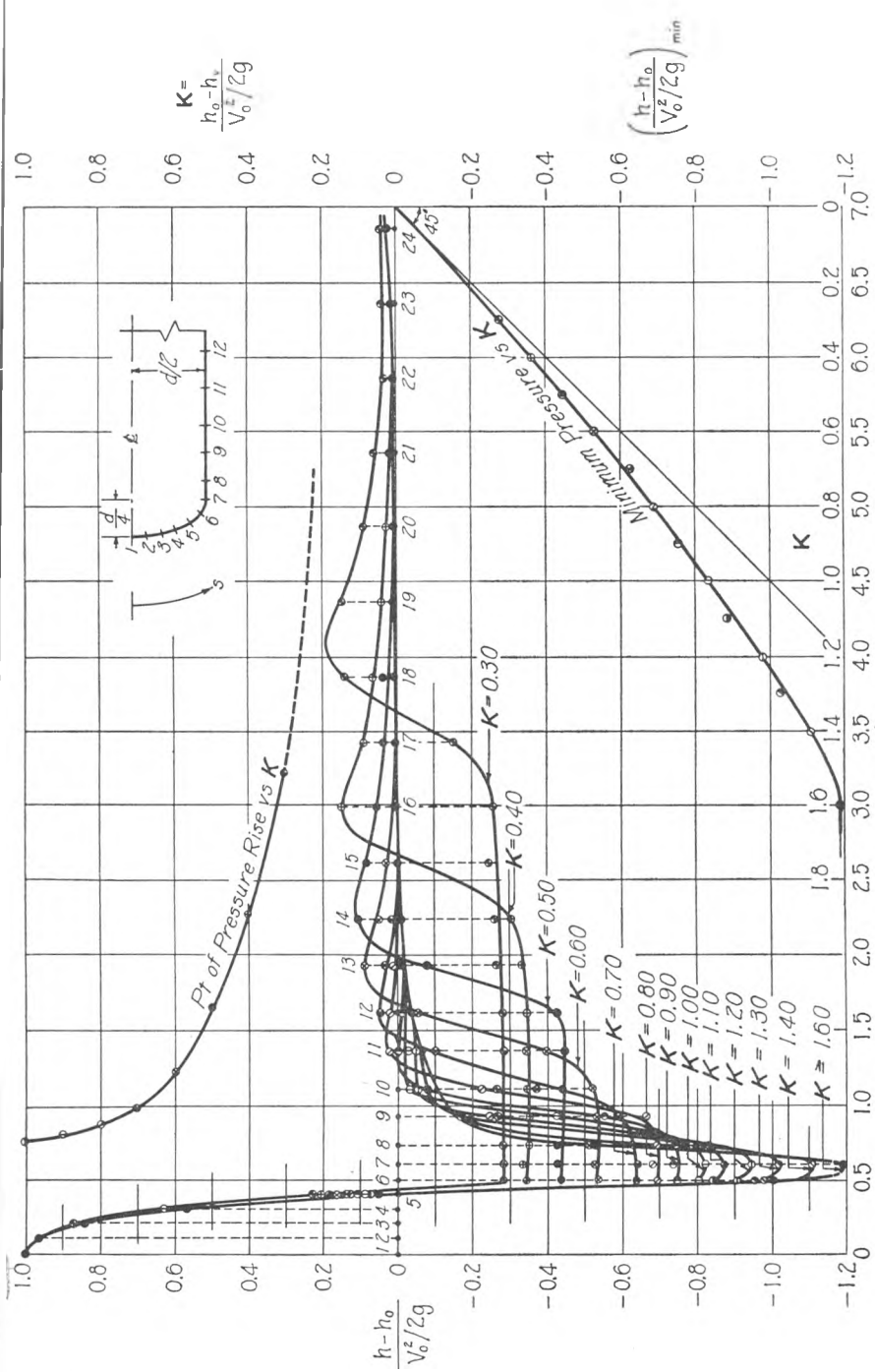

FIG. 47. EFFECT OF CAVITATION ON THE PRESSURE DISTRIBUTION AROUND A CYLINDRICAL BODY WITH A 2½:1 ELLIPSOIDAL HEAD.

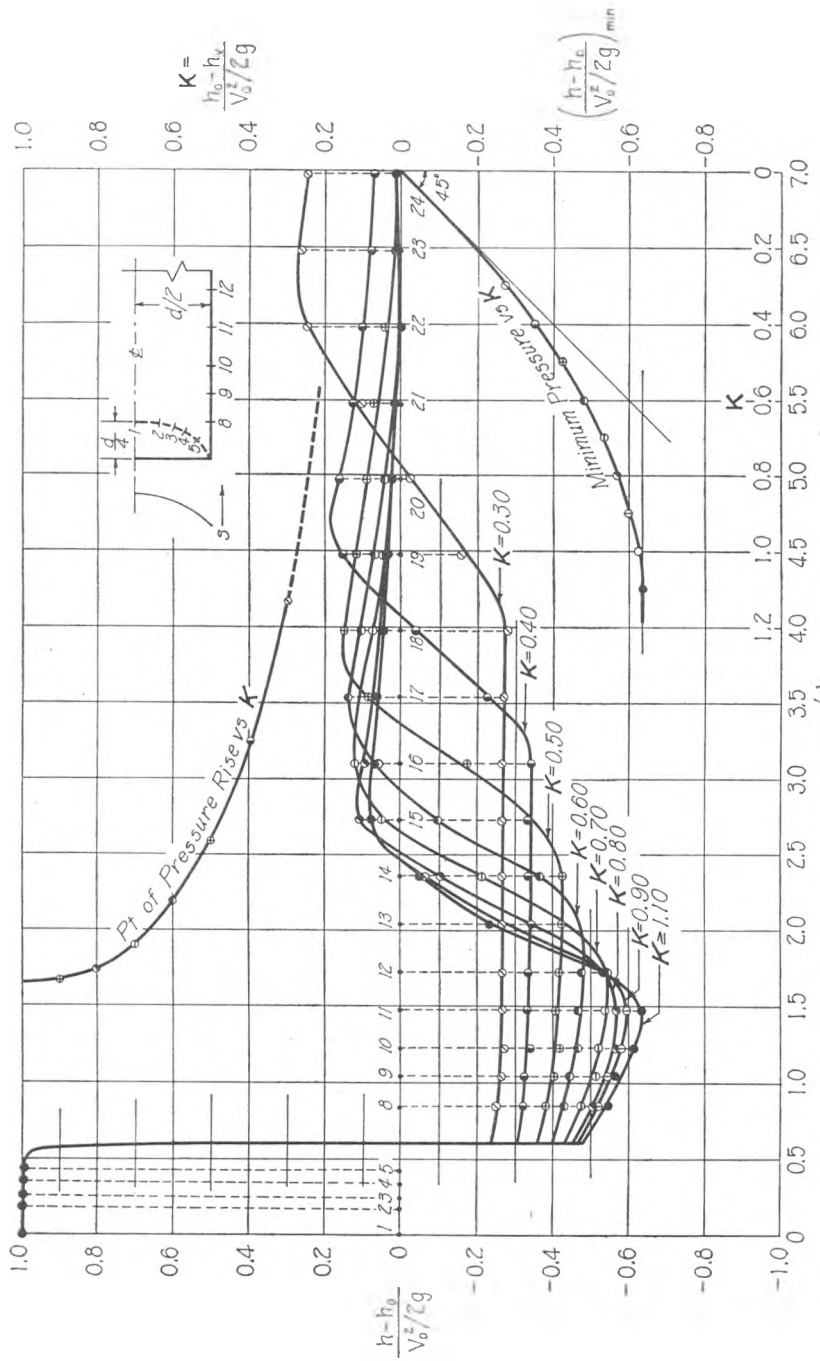

FIG. 48. EFFECT OF CAVITATION ON THE PRESSURE DISTRIBUTION AROUND A CYLINDRICAL BODY WITH A 2:1 CONCAVE ELLIPSOIDAL HEAD.

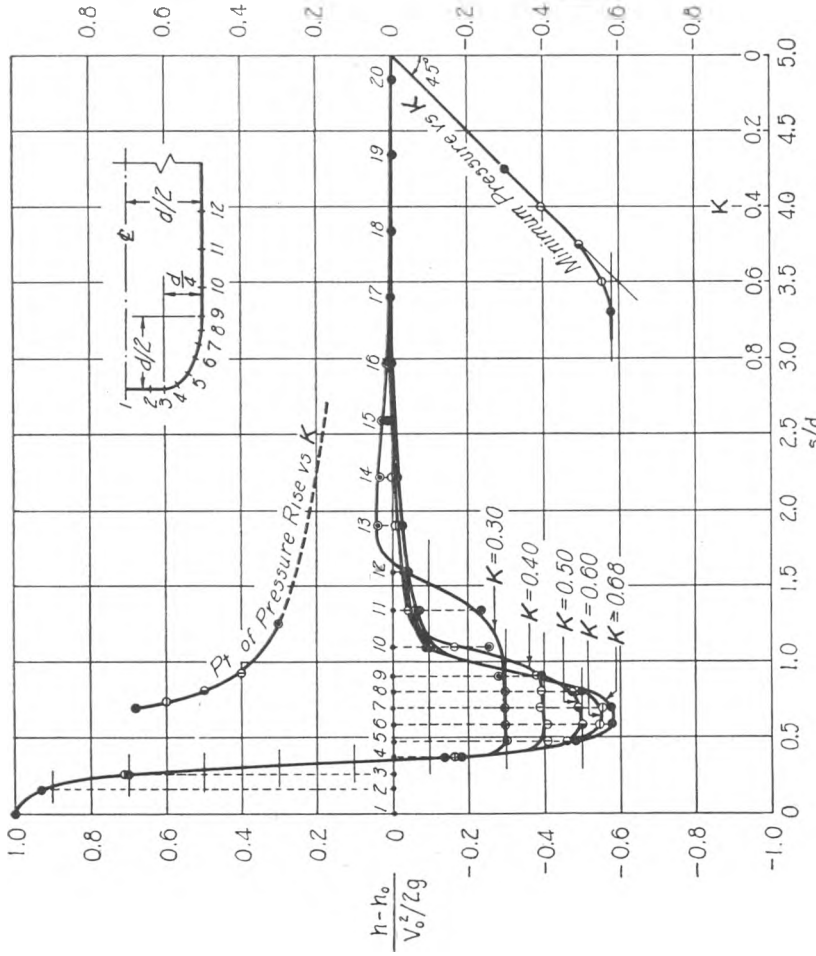

FIG. 49. EFFECT OF CAVITATION ON THE PRESSURE DISTRIBUTION AROUND A CYLINDRICAL BODY WITH A 2:1 MODIFIED-ELLIPSOIDAL HEAD.

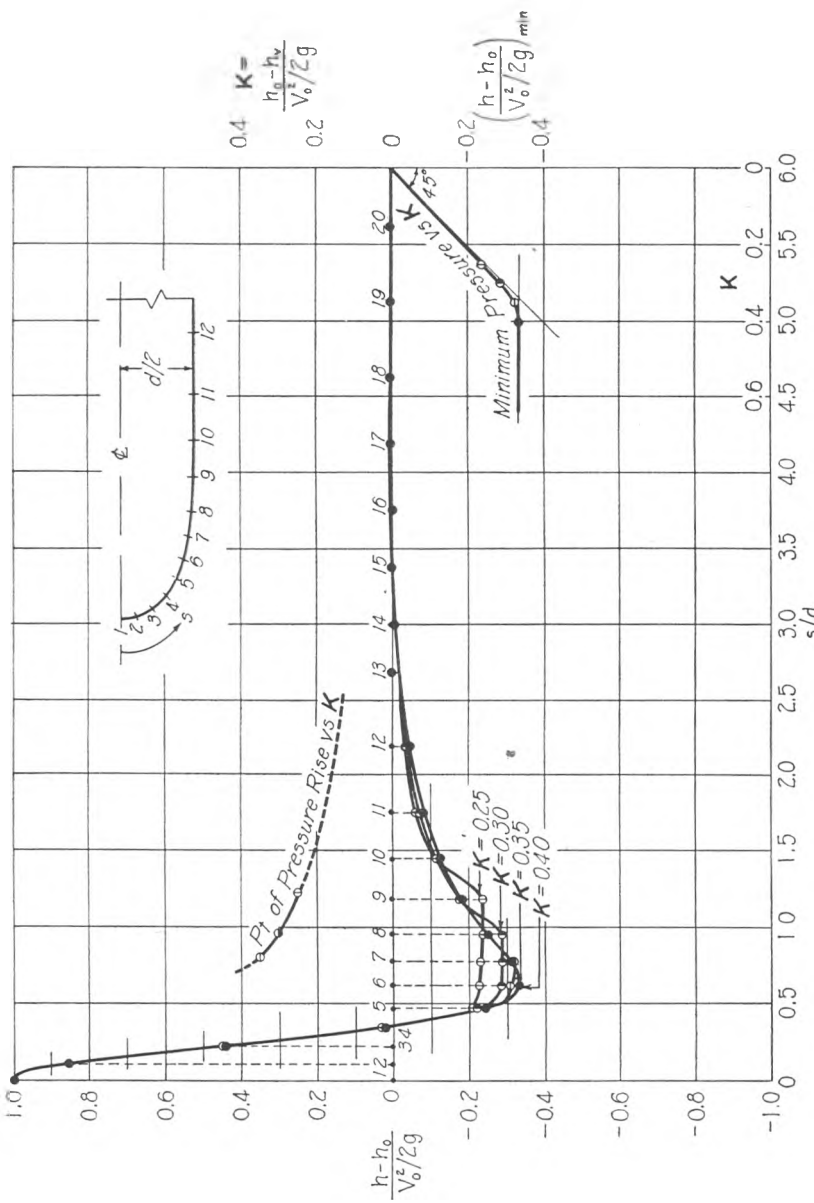

FIG. 50. EFFECT OF CAVITATION ON THE PRESSURE DISTRIBUTION AROUND A CYLINDRICAL BODY WITH A HALF-BODY HEAD.

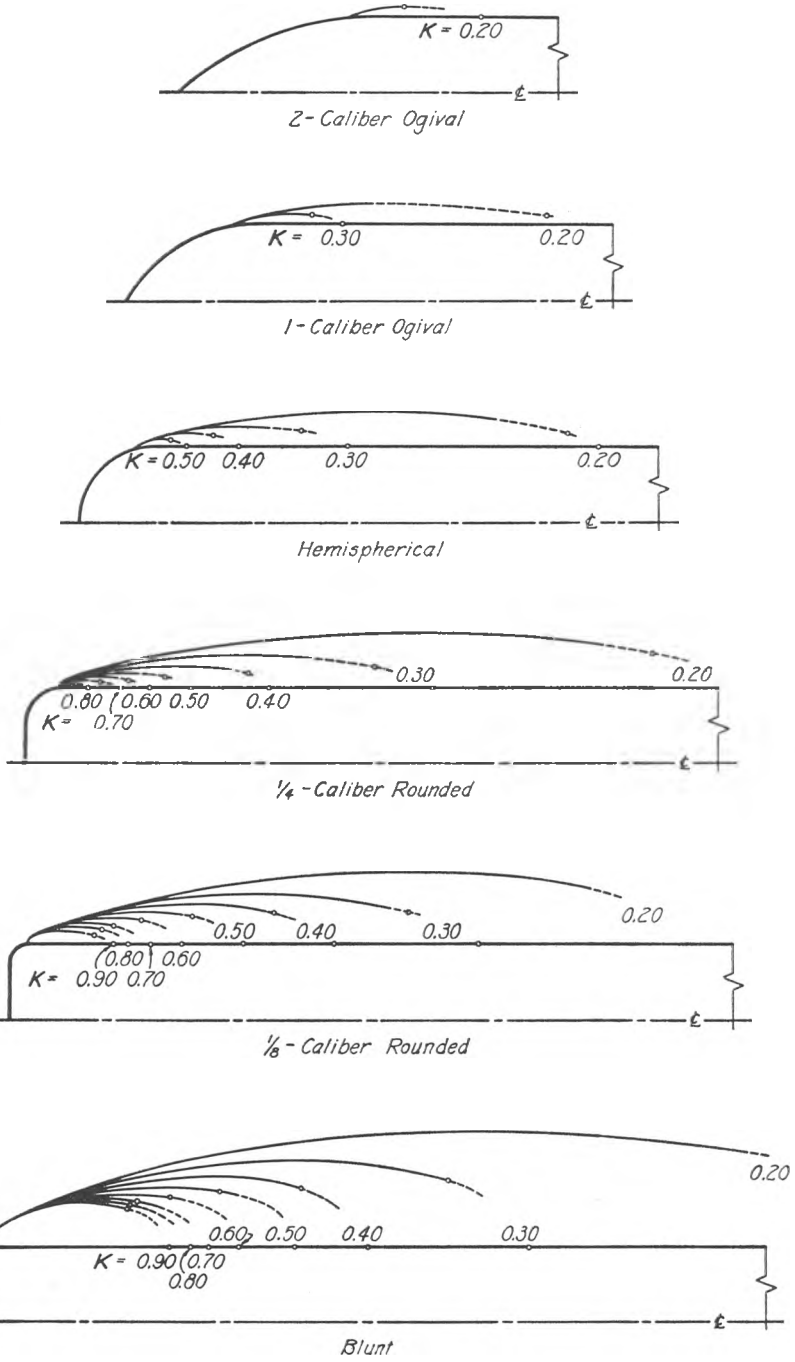

FIG. 51. MEAN CAVITATION POCKETS FOR ROUNDED HEAD FORMS, SHOWING POINTS OF INITIAL PRESSURE RISE AND APPROXIMATE END OF POCKET.

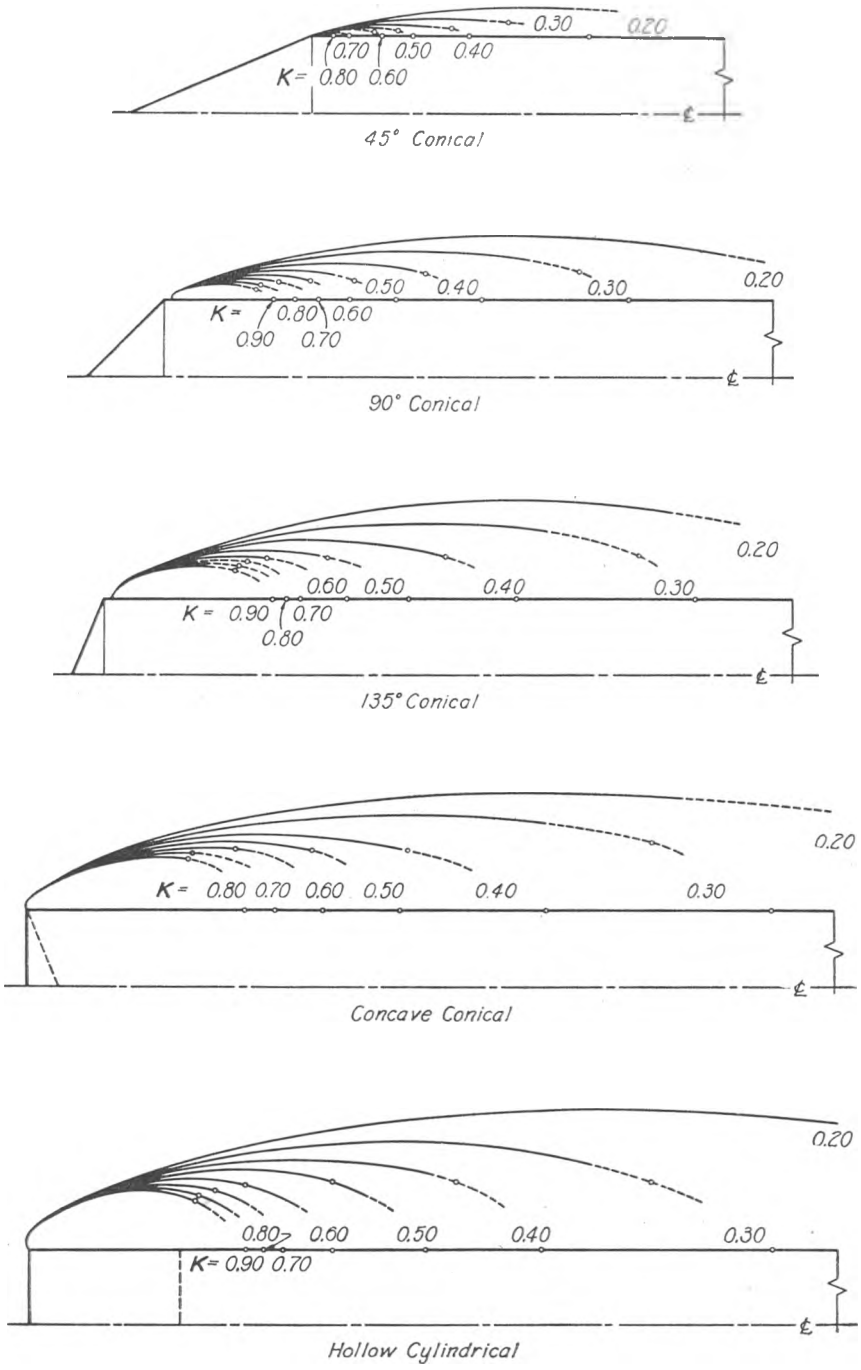

FIG. 52. MEAN CAVITATION POCKETS FOR CONICAL HEAD FORMS, SHOWING POINTS OF INITIAL PRESSURE RISE AND APPROXIMATE END OF POCKET.

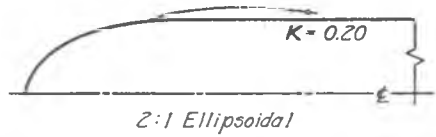

2 : 1 Ellipsoidal

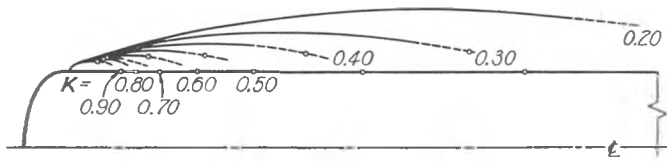

½ : 1 Ellipsoidal

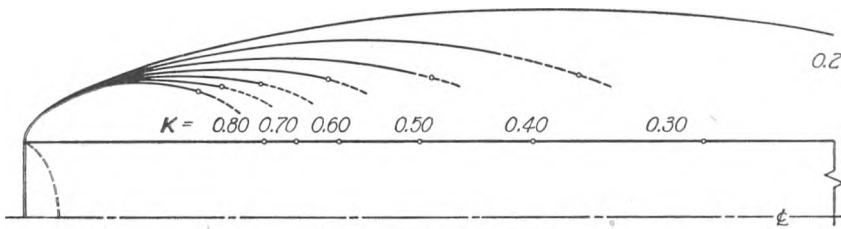

½ : 1 Concave Ellipsoidal

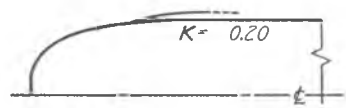

2⅔ : 1 Modified Ellipsoidal
a-d

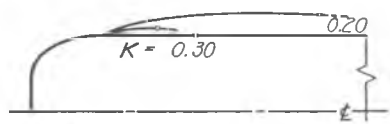

2 : 1 Modified Ellipsoidal
a-d/2

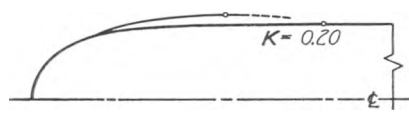

Half-Body

FIG. 53. MEAN CAVITATION POCKETS FOR ELLIPSOIDAL AND OTHER HEAD FORMS, SHOWING POINTS OF INITIAL PRESSURE RISE AND APPROXIMATE END OF POCKET.

COLLEGE OF ENGINEERING
STATE UNIVERSITY OF IOWA

Complete undergraduate courses are offered in Chemical, Civil, Commercial, Electrical, and Mechanical Engineering, as well as graduate courses in these fields and in Mechanics and Hydraulics. For detailed information, application may be made to T. H. McCarrel, Registrar.

IOWA INSTITUTE OF HYDRAULIC RESEARCH

The Institute was organized to coordinate the talents and facilities available at the State University of Iowa for the investigation of problems in the fields of fluid mechanics, hydrology, and hydraulic engineering. Through this medium the University has cooperated with government agencies, technical societies, and industrial concerns throughout the country. Correspondence regarding the services of the Institute should be addressed to Hunter Rouse, Director.

STUDIES IN ENGINEERING

Bulletin 1. The Flow of Water Through Culverts, by D. L. Yarnell, F. A. Nagler, and S. M. Woodward, 1926. 128 pages, 26 figures, 23 plates. Out of print.

Bulletin 2. Laboratory Tests on Hydraulic Models of the Hastings Dam, by Martin E. Nelson, 1932. 72 pages, 40 figures. Out of print.

Bulletin 3. Tests of Anchorages for Reinforcing Bars, by Chesley J. Posey, 1933. 32 pages, 18 figures, price $0.50.

Bulletin 4. The Physical and Anti-Knock Properties of Gasoline Blends, by Theodore R. Thoren, 1934. 32 pages, 13 figures, price $0.35.

Bulletin 5. The Transportation of Detritus by Flowing Water—I, by F. T. Mavis, Chitty Ho, and Yun-Cheng Tu, 1935. 56 pages, 15 figures, price $0.50.

Bulletin 6. An Investigation of Some Hand Motions Used in Factory Work, by Ralph M. Barnes, 1936. 60 pages, 22 figures. Out of print.

Bulletin 7. A Study of the Permeability of Sand, by F. T. Mavis and Edward F. Wilsey, 1936. 32 pages, 12 figures, price $0.35.

Bulletin 8. Radiation Intensities and Heat-Transfer in Boiler Furnaces, by Huber O. Croft and C. F. Schmarje, 1936. 32 pages, 17 figures, price $0.35.

Bulletin 9. A Summary of Hydrologic Data, Ralston Creek Watershed, 1924-35, by F. T. Mavis and Edward Soucek, 1936. 72 pages, 25 figures, price $0.50.

Bulletin 10. Report on Hydraulics and Pneumatics of Plumbing Drainage Systems—I, by F. M. Dawson and A. A. Kalinske, 1937. 32 pages, 5 figures, price $0.35.

Bulletin 11. The Transportation of Detritus by Flowing Water—II, by F. T. Mavis, Te-Yun Liu, and Edward Soucek, 1937. 32 pages, 8 figures, price $0.35.

Bulletin 12. Studies of Hand Motions and Rhythm Appearing in Factory Work, by Ralph M. Barnes and Marvin E. Mundel, 1938. 64 pages, 24 figures. Out of print.

Bulletin 13. Hydraulic Tests of Small Diffusers, by F. T. Mavis, Andreas Luksch, and Hsi-Hou Chang, 1938. 32 pages, 16 figures, price $0.25.

Bulletin 14. A Study in Flood Waves, by Elmer E. Moots, 1938. 32 pages, 7 figures, price $0.25.

Bulletin 15. The Road Map of Hydraulic Engineering in Iowa, by E. W. Lane and Edward Soucek, 1938. 16 pages, 4 figures, price $0.25.

Bulletin 16. A Study of Hand Motions Used in Small Assembly Work, by Ralph M. Barnes and Marvin E. Mundel, 1939. 68 pages, 33 figures, price $0.50.

Bulletin 17. A Study of Simultaneous Symmetrical Hand Motions, by Ralph M. Barnes and Marvin E. Mundel, 1939. 40 pages, 15 figures, price $0.40.

Bulletin 18. Percolation and Capillary Movements of Water Through Sand Prisms, by F. T. Mavis and Tsung-Pei Tsui, 1939. 32 pages, 13 figures, price $0.25.

Bulletin 19. Two Decades of Hydraulics at the University of Iowa, Abstracts of Theses, Publications, and Research Reports, 1919-1938, edited by F. T. Mavis, 1939. 84 pages, price $0.50.

Bulletin 20. Proceedings of Hydraulics Conference, edited by J. W. Howe, 1940. 260 pages, 84 figures. Out of print.

Bulletin 21. Studies of One- and Two-Handed Work, by Ralph M. Barnes, Marvin E. Mundel, and John M. MacKenzie, 1940. 68 pages, 31 figures, price $0.50.

Bulletin 22. The Study of the Effect of Practice on the Elements of a Factory Operation, by Ralph M. Barnes and James S. Perkins with the assistance and collaboration of J. M. Juran, 1940. 96 pages, 34 figures, price $0.75.

Bulletin 23. An Annotated Bibliography of Fishways, by Paul Nemenyi, 1941. 72 pages, 12 figures, price $0.50.

Bulletin 24. An Investigation of Fishways, by A. M. McLeod and Paul Nemenyi, 1941. 64 pages, 15 figures, 6 plates, price $0.50.

Bulletin 25. The Electrostatic Effect and the Heat Transmission of a Tube, by Melvin R. Wahlert and Huber O. Croft, 1941. 40 pages, 10 figures, price $0.40.

Bulletin 26. Investigations of the Iowa Institute of Hydraulic Research, 1939-1940, edited by J. W. Howe, 1941. 64 pages, 15 figures, price $0.40.

Bulletin 27. Proceedings of the Second Hydraulics Conference, edited by J. W. Howe and Hunter Rouse, 1943. 352 pages, 167 figures. Out of print.

Bulletin 28. The Preparation of Stoker Coals from Iowa Screenings, by H. L. Olin, 1942. 64 pages, 22 figures, price $0.50.

Bulletin 29. Study of Transportation of Fine Sediments by Flowing Water, by A. A. Kalinske and C. H. Hsia, 1945. 40 pages, 18 figures, price $0.40.

Bulletin 30. The Iowa Institute of Hydraulic Research. 80 pages, 36 figures, price $0.50.

Bulletin 31. Proceedings of the Third Hydraulics Conference, edited by J. W. Howe and J. S. McNown, 1947. 332 pages, 163 figures, price $2.50.